Vacuum 205 (2022) 111414

Contents lists available at ScienceDirect

Vacuum

journal homepage: www.elsevier.com/locate/vacuum

Sticking coefficient and Si/C ratio of silicon carbide growth species on reconstructed 4H – SiC$(000\bar{1})$ surface by ab-initio calculations

Ahmed Abubakar Alao [a], Weng-Ngai Wu [a], Wen-Dung Hsu [a,b,c,*]

[a] Department of Materials Science and Engineering, National Cheng-Kung University, Taiwan
[b] Hierarchical Green-Energy Materials (Hi-GEM) Research Center, National Cheng Kung University, Tainan, 70101, Taiwan
[c] Program on Semiconductor Packaging and Testing, Academy of Innovative Semiconductor and Sustainable Manufacturing, National Cheng Kung University, Tainan, 701, Taiwan

ARTICLE INFO

Keywords:
Silicon carbide growth species
Reconstructed π-bonded chain surface
Sticking coefficient
First-principles calculation
Si/C ratio

ABSTRACT

The production of silicon carbide boule for electronic device fabrication is bedeviled by defects and requires the usage of stable, high symmetry, and high-quality substrate, as a seed, for growth morphology dictation. Aside from this, process parameters such as Si/C ratio, growth temperature, and etching play certain roles in polytype stability and defect control. In this work, we estimated the Si/C ratio in the physical vapor transport process (PVT), by first, modeling and investigating several types of 4H–SiC substrates, including ideal (1x1), buckled (2x1), and (2x1) periodic π-bonded chain structures (both Si-face and C-face), via density functional theory, and found the C-face of the 4H–SiC substrate as the most stable among others. On this substrate, silicon carbide growth species get adsorb, stick, and grow, to form large SiC boule (ingot) in the PVT process. In order to have an idea of the defect concentration in the silicon carbide boule, we calculated the Si/C ratio, by estimating the sticking coefficient of individual growth contributing species ($Si_{(g)}$, $SiC_{2(g)}$, $SiC_{(g)}$, $Si_2C_{(g)}$, $Si_2C_{2(g)}$, $Si_4C_{2(g)}(I_1)$ and $Si_4C_{2(g)}(I_2)$), coupled with their concentrations. The calculated theoretical sticking coefficients for the growth contributing species at 2186 K are respectively, 0.02882, 0.01226, 0.02113, 0.01271, 0.00807, 0.00335 and 0.00433.

1. Introduction

Silicon carbide (SiC) is a semiconductor material in high demand in the foreseeable future, especially in the areas of high power and high-temperature device applications [1–3]. Conventionally, silicon has been used for most device fabrication and applications; however, it is not the best choice/option for all kinds of semiconductor applications. Therefore, the need to synthesize other semiconductor materials suitable for specific or unique applications, such as semiconductor carbide (SiC) for high power and high-temperature devices and gallium nitride (GaN) for high frequency (RF) devices is required. Silicon carbide synthesis for single crystal growth is most suitable via vapor phase epitaxy (physical vapor transport), as SiC does not have a molten state in the ambient pressure under a reasonable processing temperature. It can be synthesized through the PVT process in a controlled environment, at a temperature of around 2200 °C [4–6] and ambient pressure of $5.0\,x\,10^{-6}$ torr [7–9]. The presence of defects due to the polymorph of SiC crystal makes the synthesis of silicon carbide arduous and frustrating.

The major reason for defect formation in grown silicon carbide boule isn't impurity gasses or particles, but rather, deficiency of carbon, as its sources are only from the silicon carbide source, crucible wall (graphite), and the carbon-containing species' sublimation temperature is much higher than that of silicon's. In silicon carbide 4H–SiC homoepitaxial layer growth [10], the origin of surface defects is attributed to two aspects: (i) the propagation of substrate defects, such as inclusion, scratches, dislocation, and (ii) improper process parameters during epitaxial growth, such as Si/C ratio, growth temperature, and in-situ etch. Si/C ratio as reported is an extremely important growth parameter, and the best surface morphology is obtained under a fixed range [10]. When the ~~Si/C ratio is very low, surface morphological defects such as triangular defects could easily be grown~~ [10] and this promotes Si-vacancy (V_{Si}) [11,12]. Conversely, ~~too high Si/C ratio results in the grown crystal surface suffering from the formation of severe large steps (macro steps)~~ [10], C-vacancy (V_C) [11,12] and Si droplets [10]. In the physical vapor transport (PVT) process, the source to substrate distance

硅空位

夹杂物/划痕/错位

碳空位与硅液滴

* Corresponding author. Department of Materials Science and Engineering, National Cheng-Kung University, Taiwan.
E-mail address: wendung@mail.ncku.edu.tw (W.-D. Hsu).

https://doi.org/10.1016/j.vacuum.2022.111414
Received 11 April 2022; Received in revised form 13 July 2022; Accepted 11 August 2022
Available online 18 August 2022

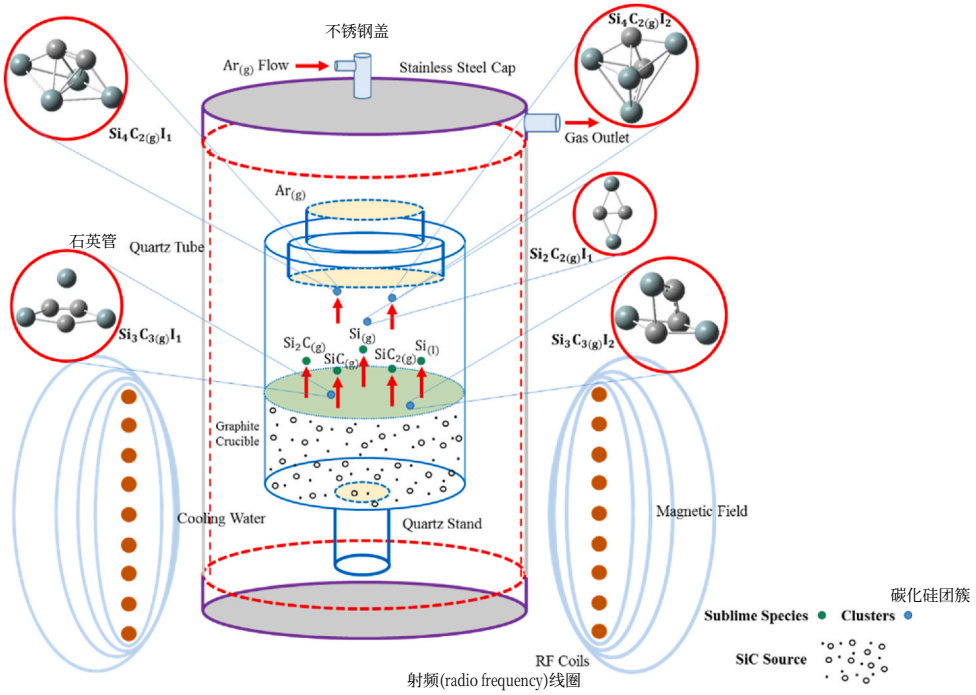

Fig. 1. Schematic representation of silicon carbide growth species, showing dominance as molecules approaches the substrate.

plays a certain role in defect concentration and crystal quality (diffusion time/space). If the source to substrate distance is placed quite far apart, sublime species from the SiC source will have enough space to diffuse ideally, and at reduced temperature (in the growth chamber), they cease to behave ideally by colliding with the graphite crucible wall, and laterally interact with each other, forming larger silicon carbide molecules (clusters). In contrast, if the source to substrate distance is maintained relatively close to each other, in such a way that, the sublime species only maintain their ideal behavior; therefore the amount of silicon gas flux will be high, thereby resulting in a non-stoichiometric ratio (非化学计量比) of silicon and carbon (high defect around carbon area, in silicon deposits). The former configuration allows species the chance to collide with the graphite crucible walls and to laterally interact, thereby forming compounds of carbon. This led to an investigation of the reaction kinetics in Ref. [13], and a pictorial summary of their findings, showing the configuration of the most dominant species in the SiC PVT process is presented in Fig. 1. It is important to consider these species, especially those molecules in which the proportion of silicon and carbon is not equal, to determine the defect ratio in the system.

In the Physical Vapor Transport (PVT) setup, a substrate or seed is required, whose size is greater than the critical nuclei radius (临界核半径). This is to provide a nucleation site (成核半径) for crystal growth. Substrates are usually sliced from large ingots, in a process known as sewing. Sewing leaves micron-size roughness (微观尺度粗糙), and thus, must be polished in a process referred to as lapping (研磨). Silicon carbide has sp3 hybridization (sp3杂化轨道), implying each silicon bonded to four carbon atoms or vice versa. This means on the substrate surface, dangling bonds (悬空键) exist, as the topmost surface atoms have no capped atoms leaving behind incomplete sp3 hybridization or dangling atoms. Each dangling atom has an unpaired electron (free electron) and is covalently paired with three electrons from three neighboring atoms, making the substrate surface act metallic rather than behaving semiconducting. Most often, atmospheric oxygen passivates (钝化) the surface, by reacting with the surface atoms to form an oxide layer (SiO2) [14–16]. This oxide layer must be knocked off via a sputtering machine, in order to provide a passivation-free surface, for growth contributing atoms/molecules to deposit, stick, nucleate and grow. However, after the sputtering process (溅射工艺), the substrate surface is mostly damaged, and therefore needs to be annealed or baked for two reasons, (i) surface reconstruction for enhancement of stability, and (ii) adhesive forces manipulation in order to improve sticking. The substrate bottom hybridization is also incomplete (sp^2) after sewing thus containing dangling bonds on the surface. Stabilization of the substrate is much needed, so as to reduce its energy, and this is achieved via either dry passivation (plasma) or wet-chemical passivation, using $H_{2(l,g)}$, $NH_{3(g)}$, $H_2S_{(g)}$ or $H_2O_{(l)}$ [18,19], in order to make a hydrogen bond with the bottom side of the substrate surface.

热退火/烘烤

Aside from the PVT configuration, building the right substrate (seed layer) plays an important role in surface adhesion (sticking) of these molecules and surface misalignment (defects or dislocation) (错位). For sp^3-hybridized substrates, K. C. Pandey [20] first predicted a stable (2 × 1) π-bonded chain structure for Si (111) surface. Thereafter, a density functional theory investigation on the reconstruction of the $4\mathbf{H}-\mathbf{SiC}(0001)_{\mathbf{Si}}$ surface was reported by Olander J and Larsson K [21], in which a conclusion of (2x1) periodicity of the $4\mathbf{H}-\mathbf{SiC}(0001)_{\mathbf{Si}}$ surface was made after optimization, where they observed each second silicon atom of the topmost layer was raised above the other ones (first silicon atoms). However, this was later refuted experimentally via molecular beam epitaxy (MBE) [22] and was termed a buckled (2x1) surface of the $4\mathbf{H}-\mathbf{SiC}(0001)_{\mathbf{Si}}$ face, since it is indistinguishable from the ideal (1x1) model through LEED or RHEED pattern. An in-situ observation of the $4\mathbf{H}-\mathbf{SiC}(0001)_{\mathbf{Si}}$ surface placed in the MBE system shows 2-fold and 1-fold bright symmetry along $(11\bar{2}0)$ and $(1\bar{1}00)$ azimuth respectively, when viewed on a reflection high-energy electron diffraction screen (RHEED), indicating a (2x1) periodic reconstruction. The same conclusion was also deduced in Ref. [23], where cleave surfaces of silicon carbide $6\mathbf{H}-\mathbf{SiC}(0001)_{\mathbf{Si}}$ and $\mathbf{SiC}(000\bar{1})_{\mathbf{C}}$ were examined using low-energy electron diffraction (LEED) and core-level photoelectron spectroscopy (PES). It was deduced that, flat surfaces of $6\mathbf{H}-\mathbf{SiC}(0001)_{\mathbf{Si}}$ and $\mathbf{SiC}(000\bar{1})_{\mathbf{C}}$ are obtained in LEED pattern as sharp, and interpreted as a 3-domain superposition of (2x1) reconstructions based on spot intensity differences. Since there is a similarity in structure between 6H–SiC and 4H–SiC (both hexagonal), and the energy difference is quite small, Tomoaki Kaneko et al. [24] investigated the surface reconstruction behavior of 4H–SiC surfaces and observed the (2x1) π-bonded chain structure as the most stable.

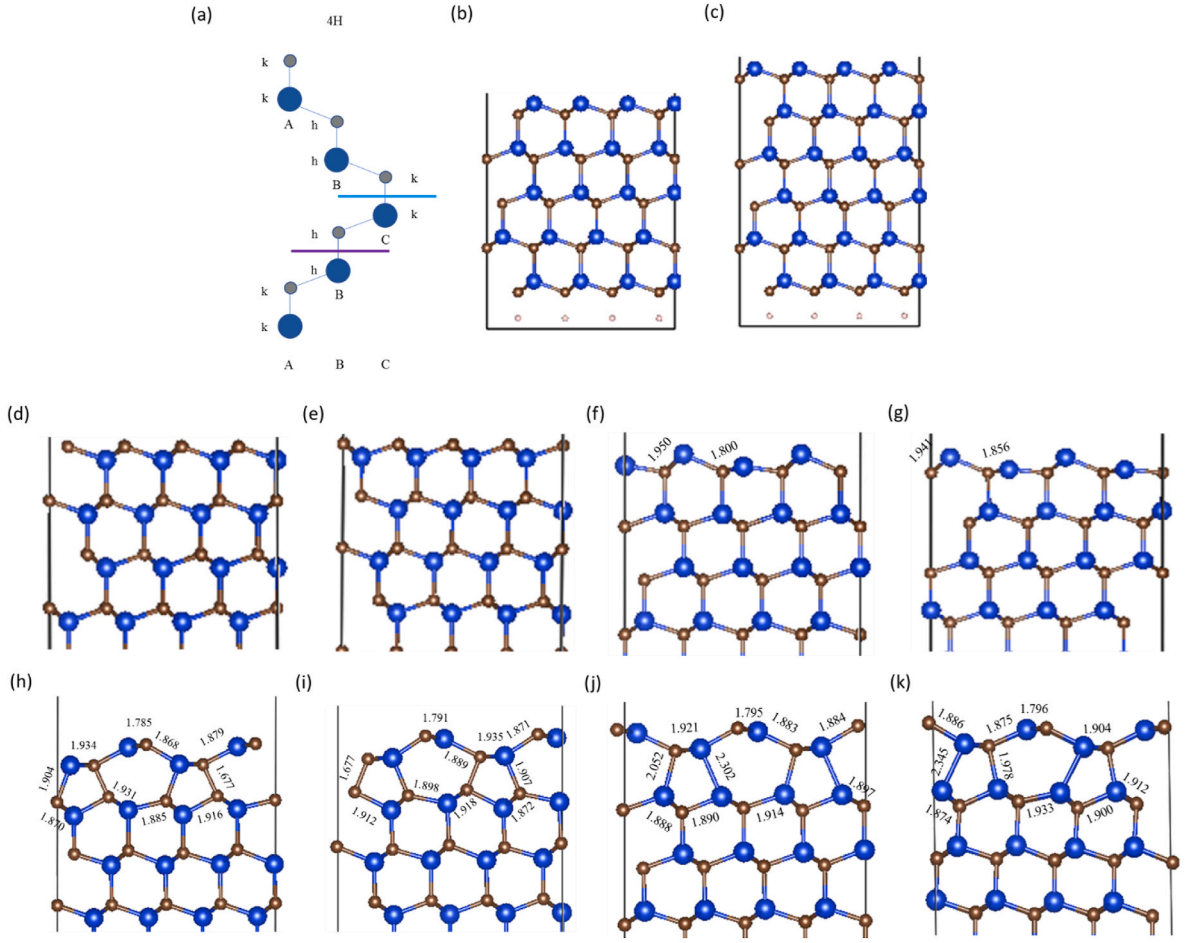

Fig. 2. (a) The stacking sequence of 4H–SiC polytype, indicating Si (blue ball) and C (ash ball) atoms. The light blue and purple planes indicate the two inequivalent terminations in 4H–SiC, h-termination, and k-termination respectively. (b) Ideal (1 × 1) 4H − $SiC(0001)_{Si}$ k-like stacking with hydrogen passivation. (c) Same model as (b), but h-like stacking. (d) Ideal (1 × 1) 4H − $SiC(000\bar{1})_{C}$ k-like stacking with hydrogen passivation. (e) Same figure as (d) for the h-like stacking. (f) Buckled model of 4H − $SiC(0001)_{Si}$ with k-like stacking and (2 × 1) top surface periodicity. (g) Same figure as (f) but, for the h-like stacking. (h) 4H − $SiC(000\bar{1})_{C}$ π-bonded chain (π-BC) model, with (2 × 1) periodicity and k-like stacking. (i) Same figure as (h) for the h-like stacking. (j) 4H − $SiC(0001)_{Si}$ π-bonded chain (π-BC) model, with (2 × 1) periodicity and k-like stacking. (k) Same figure as (j) for the h-like stacking.

In this research work, we employed the ab-initio method, to model the (2 × 1) reconstructed 4H–SiC π-bonded chain structure and other surfaces in order to investigate their stability. Subsequently, we estimate the Si/C ratio by calculating the sticking coefficients based on the adsorption energies and possible adsorption sites. The results could provide the optimal condition for the PVT process.

2. Theoretical methods

The 4H − $SiC(000\bar{1})_{C}$ (carbon surface) and 4H − $SiC(0001)_{Si}$ (silicon surface) substrate models investigated in this study were built via VESTA, by first examining the reported theoretical and experimental atomic behavior of the substrates as explained in the prior section. We, therefore, mimic this by utilizing VESTA to first build a unit cell of 4H − SiC. Then the slab models were created by duplicating the original unit cell via transformation into an arbitrary integer multiple of the original unit cell. For the case of 4H − $SiC(000\bar{1})_{C}$ and 4H − $SiC(0001)_{Si}$ slab models, internal planes of $(000\bar{1})$ and (0001) were selected as the exposed surface of the carbon and silicon face respectively, while the ***b*** and ***a*** vectorial axis were chosen as (2 × 1) periodicity, representing $[1\bar{1}00]$ and $[11\bar{2}0]$ directions. Thereafter, the dimensionality of the slab models is changed by transforming them into supercells of size (2 × 3 × 2) and (3 × 2 × 2) for (2 × 1) periodic models of 4H− $SiC(0001)_{Si}$ and 4H − $SiC(000\bar{1})_{C}$, respectively. Whilst for the (1 × 1) ideal models, supercell size of (3 × 4 × 2) was used for both the Si and C face. The direction of the $a[1\bar{1}00]$ and $b[11\bar{2}0]$ sides of the substrate are preserved to mimic the real situation by keeping the periodicity in these directions, while a vacuum distance of 15 Å is included in the *c*-axis. Due to the inequivalence of the 4H–SiC planes perpendicular to the surface, the Jagodzinski [25] h–k notation is used to assign the surface termination (A-B-C-B for k-site stacking and B-A-B-C for h-site stacking as shown in Fig. 2(a)).

广义梯度近似 (GGA)

The slab models are then optimized using first-principles calculations based on density functional theory [26,27], within the generalized gradient approximation (GGA) [28] (Perdew-Burke-Ernzerhof). The commercially available package, Vienna *ab initio* simulation package (VASP) was used to obtain the electronic structures of all the models and their energies. This software solves Kohn and Sham equations by utilizing the projector-augmented wave (PAW) method [29,30] for the interactions between ionic cores and valence electrons. This is usually coupled with periodic boundary conditions, plane-wave basis set, and a generalized gradient approximation (GGA) with parameterization of Perdew-Burke-Ernzerhof (PBE) for the exchange-correlation functional [31]. For the bulk 4H − SiC, substrate models (adsorbent) and adsorbed molecules (adsorbate), a converged plane wave cut-off energy of 500 eV was used [32], which yield optimized bulk lattice constants of a = 3.09 Å, b = 3.09 Å and c = 10.13 Å, which are in good agreement with

投影缀加波（赝势

近似的能量泛函

Table 1
Spin-polarized and un-polarized optimized structures of 4H− SiC substrates, featuring (1 × 1) ideal k and h-like stacking and (2 × 1) π-bonded chain (π-BC) models of k and h-like stacking.

Si-/C (Face) (k/h)	Model	Energy (eV) Un-polarized	Energy (eV) Spin-Polarized	Rel. Energy (eV) Un-polarized	Rel. Energy (eV) Spin-Polarized
Si-face (h)	(1 × 1) Ideal	−1091.6035	–	0.0000	–
	(2 × 1) π- BC	−1095.0299	–	−3.4264	–
Si-face (k)	(1 × 1) Ideal	−911.0482	−912.2390	0.0000	−1.1908
	(2 × 1) π- BC	−916.3942	–	−5.3460	–
C-face (h)	(1 × 1) Ideal	−1074.8548	–	0.0000 (16.7487)	0.000
	(2 × 1) π- BC	−1103.4580	–	−28.6032 (−8.4281)	–
C-face (k)	(1 × 1) Ideal	−896.2162	−898.2545	0.0000 (14.8320)	−2.0383 (13.9845)
	(2 × 1) π- BC	−922.4569	–	−26.2407 (−6.0627)	–

experimental values [33,34]. In all the substrate and adsorbate models, the Brillouin zone integration was sampled on a Monkhorst-Pack k-point grid and Γ-centered [35], in order to set the mesh position at the center of the zone. Γ-centered (4 × 6 x 1) mesh points were sampled for supercell (2 × 3 x 2) for 4H − $SiC(0001)_{Si}$ Si-face(k) and Si-face(h), and a Γ-centered (6 × 4 x 1) sampled for (3 × 2 x 2) supercell for 4H− $SiC(000\bar{1})_{C}$ C-face(k) and C-face(h) termination. Whilst for the (3 × 4 x 2) ideal supercell model, a Γ-centered (8 × 6 x 1) k-point was sampled. It should be worth noting that, k-points along a and b axial dimensions are finite lengths and multiple of the integer values along these axis is a wise choice, but dimension along c-axis is an artifact of infinite length and 1 k-point sampling is the way to go.

For the optimization, simulations for both spin unpolarized (ideal and (π-BC) bonded structure) and polarized (ideal) calculations were performed. Moreover, an initial equilibrium adsorption distance was determined on the lowest energy π-bonded chain (π-BC) structure (C-face (h)), where values of 1.936 Å, 1.855 Å, 1.850 Å, 1.855 Å, and 2.400 Å were obtained for $\mathbf{SiC}_{(g)}$, $\mathbf{Si_2C_{2(g)}}$, $\mathbf{SiC_{2(g)}}$, $\mathbf{Si_4C_{2(g)}}(\mathbf{I_1})$ and $\mathbf{Si_4C_{2(g)}}(\mathbf{I_2})$ molecules on the surface, respectively. The GGA optimized geometries were then used in calculating the adsorption energies, using the relation: (1)

$$E_{ads} = E_{system} - (E_{adsorbent} + E_{adsorbate}) \tag{1}$$

Where $\boldsymbol{E_{ads}}$, is the adsorption energy, $\boldsymbol{E_{system}}$ is system energy comprising the adsorbent (slab) and adsorbate (molecule), $\boldsymbol{E_{adsorbent}}$ is the slab energy and $\boldsymbol{E_{adsorbate}}$ is the molecular energy. All energy units are in eV.

The sticking coefficient of species (A) (S_A), describes the probability of the gaseous species (A) to be adsorbed and stick on the surface per strike [36]. This coefficient can be calculated from one out of the following two methods: (i) Reuter and Scheffler's mathematical model of temperature-dependent sticking coefficient [37], and (ii) Molecular dynamics simulation (MD) of species impingement on the substrate [38,39]. By assigning an initial species velocity (average molecular velocity) for surface impingement, atoms/molecules could both get adsorb or desorb, and a ratio of the number of atoms/molecules adsorbed to the total number of impingement, defines the sticking coefficient. In our own investigation, we employed a modified version of Reuter and Scheffler's equation $S_A = R_{ads}/\varphi_A$ [36]. Where R_{ads} is the adsorption rate of gaseous species (A) on an atomic site (silicon/carbon) or on a bond terminated site (this can also be written as $\boldsymbol{A_{(g)} - Si_{(s)} \leftrightarrow}$ **product,** $\boldsymbol{A_{(g)} - C_{(s)} \leftrightarrow}$ **product** and $\boldsymbol{A_{(g)} - SiC_{(s)} \leftrightarrow}$ **product**, respectively). The adsorption rate is derived as $R_{ads} = f_{ads}\exp(-\Delta E_{act}/k_BT)\varphi_A$ $(molecule\ site^{-1}s^{-1})$.

Where φ_A, is the impingement rate of species (A), ΔE_{act} refers to the activation energy of the adsorption process at 0 K, T is the temperature (K), k_B is the Boltzmann constant, and f_{ads} is the phonon contribution or surface vibration of atoms which reduces the sticking probability due to the system's degree of freedom.

The modified Reuter and Scheffler's sticking coefficient, S_A, result in the Arrhenius term $S_A = f_{ads}\exp(-\Delta E_{act}/k_BT)$. However, in our investigation of adsorption of SiC species on the reconstructed 4H − $SiC(000\bar{1})_C$ π-bonded chain surface, there appears to be no energy barrier during adsorption of the species as this will be explained in the subsequent section. Since there were no barriers observed (via Nudged Elastic Band (NEB) calculation) during the adsorption of the molecules, the equation reduces to $S_A = f_{ads}$. Where $f_{ads} = \sum_i^x \beta_{P_x} f_{A_x} P_{s_x}$, is the surface vibration of atoms (phonon), and its expansive form is shown as equation (2). To obtain the numerical solution to this equation, we first utilized the calculated adsorption energies of individual sites in order to know the status of adsorption, and also calculate the Boltzmann term of individual adsorb sites ($\boldsymbol{\beta_{P_x}}$). Thereafter, for each site, we count the number of identical sites on the substrate and obtain the probability of the sites, as the ratio of the number of identical sites to the total number of substrate sites. Depending on the sticking site (be it atomic or bond), the fractional area of sticking is also accounted for, and therefore, the sticking coefficient of an individual site is derived as the product of the probability of its site, Boltzmann term of the adsorb site and the fractional area of the adsorb atom or bond on that specific site. An overall sticking coefficient (equation (2)) is derived via summation of all individual site sticking coefficients for only favorable adsorption.

$$\text{Sticking Coefficient, } (S_A) = \sum_i^x \beta_{P_i} f_{A_i} P_{s_i} + \beta_{P_j} f_{A_j} P_{s_j} + \ldots + \beta_{P_n} f_{A_n} P_{s_n} \tag{2}$$

Where $x = i, j, \ldots, n$ is the notation for sites $f_{A_x} = f_{A_i}, f_{A_j}, \ldots, f_{A_n}$ is the fractional area of the adsorb atom/bond on site x (individual fractional area), $\beta_{P_x} = \beta_{P_i}, \beta_{P_j}, \ldots, \beta_{P_n}$ is the Boltzmann probability term dependent on the adsorption energy of site (x) and temperature, and $P_{s_x} = P_{s_i}, P_{s_j}, \ldots, P_{s_n}$ is the probability of site (x) (individual sites probability). The fractional area of a site is calculated as, the ratio of the sticking surface to the total atomic/bond surface area. Boltzmann probability term on an individual adsorbed site is calculated by taking the ratio of the Boltzmann factor 玻尔兹曼因子 to the normalization constant (total partition function of the sites, $\sum_x e^{-\frac{E_{ads_x}}{k_BT}}$). As the term depends on the site's adsorption energies and temperature, the effect of temperature increase on the overall sticking coefficient of a molecule is observed to be an approximate constant, because the energy difference in the adsorption energies of the sites is quite small. Thus, it could be taken as a constant term as regards temperature increase.

$$\beta_{P_x} = \frac{e^{-\frac{E_{ads_x}}{k_BT}}}{\sum_x e^{-\frac{E_{ads_x}}{k_BT}}} \tag{3a}$$

3. Results and discussion

3.1. Models and their stability

Ab initio geometry optimizations were performed on different slab models of the 4H − SiC substrate, including (2 × 1) 4H − $SiC(000\bar{1})_C$, 4H − $SiC(0001)_{Si}$ reconstructed π-bonded chain (π-BC) models and ideal (1 × 1) Si and C-face models. Based on the experimental report, buckled model (2 × 1) periodicity is observed to be indistinguishable from the (1 × 1) ideal model and it is found to be energetically unstable compared to the former and latter models, via extensive density functional theory investigation [24]. Therefore, we exclude it from our study and

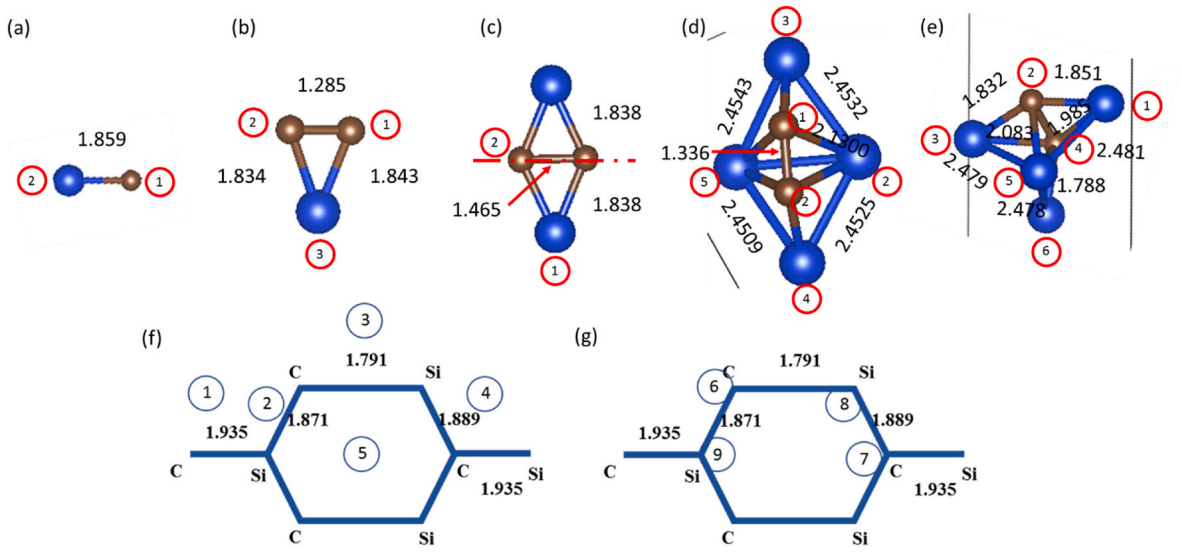

Fig. 3. Individual adsorbate sites and hexagonal surface sites of the π-bonded chain (π-BC) surface (a) $SiC_{(g)}$ sites (b) $SiC_{2(g)}$ sites (c) $Si_2C_{2(g)}(I_1)$ sites (d) $Si_4C_{2(g)}(I_1)$ sites (e) $Si_4C_{2(g)}(I_2)$ sites (f) Bond and hollow sites, and (g) On top atom sites of the $4H-SiC(000\bar{1})_C$ π-bonded chain (π-BC). All bond dimensions are given in Armstrong.

performed spin-polarized and unpolarized calculations on π-bonded chain (π-BC) models and ideal (1 × 1) Si and C-face models. In the ideal models, the top most atoms of silicon and carbon on the substrate surface are of sp^2 hybridization (bonded to three atoms), and thus contain dangling bonds. While for the π-bonded chain structures, models were built by reconstructing the topmost two bilayers of the hexagonal membered ring, in a (2 × 1) structure of Si-face and C-face, to five and seven-membered rings similar to that predicted by Pandey [40,41]. The π-bonded chain structures, after reconstruction, appear not to contain any dangling bond sites, because the Si and C atoms in the seven-membered ring are close enough spatially to form a bond (π-bond).

Fig. 2(b–k) depicts pictorial views of ideal (1 × 1) Si-face (k and h-like stacking), (1 × 1) ideal C-face (k and h-like stacking), k and h-like stacking of buckled Si-face SiC, k and h-like stacking of $4H-SiC(000\bar{1})_C$ and $4H-SiC(0001)_{Si}$ π-bonded chain (π-BC) models, respectively. Spin-polarized and un-polarized optimizations were performed on ideal models of Si and C-face, both k and h-like stacking, as shown explicitly in Table I. While for the case of π-bonded chains, only un-polarized calculations were performed because of their instability due to spin polarization, resulting in un-polarized wave functions [24]. Optimization results show among other previous findings that π-bonded chain structures, both Si and C-face (k and h-like stacking) are the most stable possible versions of the substrate. The C-face, k, and h-like stacking are more stable, with the latter being the most favorable in stability. Ideal models are second in terms of stability rankings and prefer spin-polarized calculations, as they are more energetically stable. Models of spin-polarized h-like stacking of 4H – SiC, Si, and C-faces, are somewhat difficult to converge and hence, termed unstable models of (1 × 1) ideal structures. We, therefore, retained the C-face h-like stacking, of the π-bonded chain (π-BC) model as the most stable and practically viable of the 4H – SiC substrate.

Adsorption of **SiC** growth species on the (2 × 1) $\mathbf{4H-SiC(000\bar{1})_C}$ π-bonded chain (π-BC) Surface.

For the adsorption of SiC growth species on the reconstructed π-bonded chain (π-BC) C-surface, we considered the most dominant SiC gas-phase species ($Si_4C_{2(g)}(I_1)$, $Si_4C_{2(g)}(I_2)$, $SiC_{2(g)}$ and $Si_2C_{2(g)}(I_1)$) from source sublimation, reactions resulting from the collision of sublime species with carbon crucible wall, and lateral interaction reactions reported by A. Abubakar Alao and W.-D. Hsu [13]. These species considered the most dominant (shown in Fig. 3), are also regarded as the likely SiC growth species, contributors since gas-phase dominance transport to increase the impingement rate. $SiC_{(g)}$ is inclusive for surface adsorption not that it is dominant, but because the sticking coefficient of SiC gas on SiC surfaces might be quite great. The fact that $Si_{(g)}$ and $Si_3C_{3(g)}(I_1$ & $I_2)$ species [13] are excluded from this investigation of growth contributing species, doesn't term the former as sparse, but rather, they mostly partake in producing species of $Si_4C_{2(g)}(I_1$ & $I_2)$. However, its sticking coefficient is estimated in subsequent sections for further investigations. The latter, $Si_3C_{3(g)}(I_1$ & $I_2)$ is not ample, and its adhesion or sticking coefficient on the SiC surface should be good, but its stoichiometric ratio (Si/C ratio) is 1:1. Hence, it is discarded.

While adsorbing the molecules on the substrate, three possible molecular sites on the surface (i.e. (i) Molecular atoms on top adsorption to surface atoms, (ii) Molecular bonds adsorption to surface bonds, and (iii) Molecular atoms adsorption on surface bridge sites) should be the ideal configuration. The first two configurations, respectively involve adsorbing on top molecular atoms on dissimilar surface atoms, while the second, is for adsorption of two molecular bond atoms on dissimilar surface bond atoms, except for molecular Si–Si or C–C bond adsorption. The third configuration of molecular atoms on surface bridge sites mostly converges to the first case (i). For instance, when molecular Si-atom is placed on the surface bridge (in between Si–C bond) at equilibrium adsorption distance, surface Si-atom interacts with the molecular Si-atom to form a bond (since Si–Si bond could form from a farther distance), which upon optimization converges more towards the surface Si-atom. Turning it on top Si–Si adsorption, which is unconventional to SiC formation. Likewise, when the molecular C-atom is placed on the surface bridge, the surface Si-atom interacts with the molecular C-atom to form a bond (since C–C interaction is limited at a farther distance), which when optimized, converges toward the surface Si-atom, forming an on top C–Si bond (configuration (i)). These first two aforementioned adsorption configurations are distinctive to Si–C formation (growth) and should be the applicable and ideal modeling case.

3.2. $\mathbf{SiC_{(g)}}$ *Species adsorption*

$SiC_{(g)}$ abundance in the gas phase is quite limited, however, it is considered because of its likely great sticking coefficient to the surface of $4H-SiC(000\bar{1})_C$ π-bonded chain (π-BC). For the adsorption, we first determine the number of sites on the adsorbate (SiC gas) due to its

Table 2
Molecule to surface minimum adsorption distance, system minimum energy (adsorbate on adsorbent), molecular active site's bond lengths, molecular surface binding sites, and their corresponding adsorption energies.

Molecule	Minimum Adsorption Distance (Å)	Minimum Energy (eV)	Molecular Bond Length (Å)	Surface Site	Adsorption Energy (eV)
$SiC_{(g)}$	1.936	−1114.8558	1.822	T7C_R	−5.2240
$Si_2C_{2(g)}(I_1)$	1.855	−1128.2338	1.838	Si–C_S86	−2.4562
$SiC_{2(g)}$	1.850	−1123.4259	1.843	Si–C_S86	−2.7796
$Si_4C_{2(g)}(I_1)$	1.855	−1137.7293	1.336	C–C_S68	−1.2225
$Si_4C_{2(g)}(I_2)$	2.400	−1138.1103	1.851	Si–C_S68	−2.0945

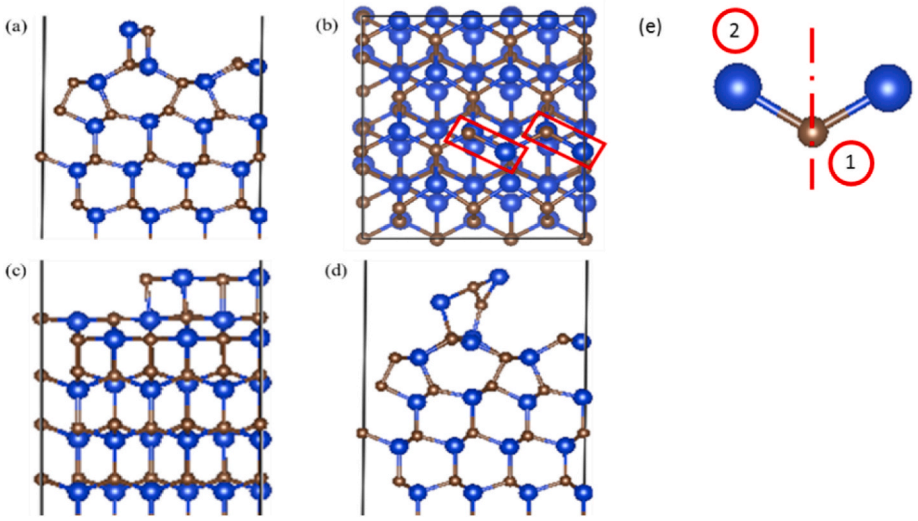

Fig. 4. Adsorption of two (2) moles of SiC on the π-bonded chain (π-BC) surface (a) Front view (b) Plan view (c) Side view (d) Adsorption of $Si_2C_{2(g)}(I_1)$ molecule (e) $Si_2C_{(g)}$ optimized geometry.

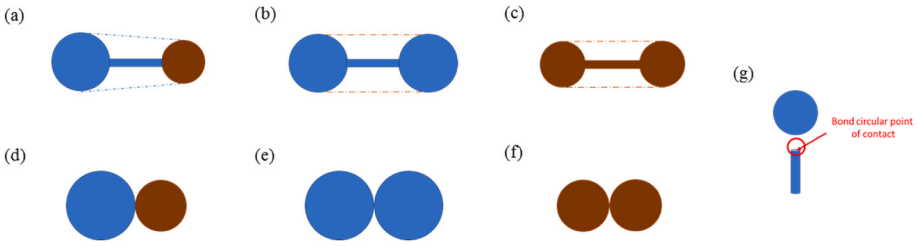

Fig. 5. Conventional bond models of (a) Si–C (b) Si–Si, and (c) C–C for surface area calculation. Hard sphere models of (a) Si–C (b) Si–Si, (c) C–C for surface area calculation, and (g) Atomic site sticking model of silicon.

Table 3
Calculated atomic/molecular area, covalent radii, molecular single bond covalent radii, equilibrium bond lengths, and fractional area.

Task/Analysis	Silicon	Carbon	Si–Si Bond		Si–C Bond		C–C Bond	
			Hard Sphere Model	Conventional Model	Hard Sphere Model	Conventional Model	Hard Sphere Model	Conventional Model
Calculated Area ($Å^2$)	15.4893	7.4536	38.7231	55.1752	28.0429	38.3481	18.634	26.0876
Surface Accessible Solvent Area (VMD-SASA)				135.1449		114.8241/ 172.4961		94.1529
Solvent						Argon/Water		
Covalent Radius (Å)	1.11 [56]	0.77 [57]						
Molecular Single Bond Covalent Radius (Å)	1.16 [58]	0.75 [59]						
Equilibrium Bond-Length (Å)				2.358 [44,45]		1.749 [46]		1.54 [47]
Fractional Area of Atom/Bond Site	0.2730	0.2372	0.2184	0.1533	0.2138	0.1564	0.1897	0.1355

Table 4
Adsorption sites, status, number of surface binding sites and sticking coefficient of SiC at 2186 K.

Atom/Bond Site	Surface Site	Site	Adsorption Status	No. of Binding Site	Probability (P_s)	Fraction of Area (f_A)	Boltzmann Term (β_P)	Site Sticking Coefficient (S_c)
Si	7	T7-R T7-L T7-V	Ads.	6	0.09091	0.2730	1.64843E-11	4.09113E-13
C	9	T9-R T9-L T9-V	Ads.	6	0.09091	0.2372	0.222510	0.004798
Si	6	T6_R T6_L T6_V	Ads.	6	0.09091	0.2730	0.000265	6.58833E-06
C	8	T8_R T8_L T8_V	Ads.	6	0.09091	0.2372	0.054790	0.001181
C on C (neighboring Si)	7	T7C_R T7C_L T7C_V	Ads.	6	0.09091	0.2372	0.636554	0.013727
SiC	79	Si–C_S79	Ads.	12	0.18182	0.1564	0.013278	0.000378
	69	Si–C_S96	Ads.	6	0.09091	0.1564	0.071826	0.001021
	68	Si–C_S68	Ads.	12	0.18182	0.1564	0.000776	2.2059E-05
	78	Si–C_S87	Ads.	6	0.09091	0.1564	1.64843E-11	2.34378E-13
	Sticking Coefficient	0.021134						

Table 5
Adsorption sites, status, number of surface binding sites and sticking coefficient of $SiC_{2(g)}$ at 2186 K.

Atom/Bond Site	Surface Site	Site	Adsorption Status	No. of Binding Site	Probability (P_s)	Fraction of Area (f_A)	Boltzmann Term (β_P)	Site Sticking Coefficient (S_c)
1	8	C1-8L C1–8V C1-8R	Ads.	6	0.04167	0.2372	0.128627	0.001271
	9	C1–9V C1-9R	Ads.	6	0.04167	0.2372	0.000106	1.05046E-06
2	8	C2-8L C2–8V C2-8R	Ads.	6	0.04167	0.2372	0.084566	0.000835
	9	C2–9V C2-9R	Ads.	6	0.04167	0.2372	0.000478	4.73386E-06
3	6	Si-6L Si–6V Si-6R	Ads.	6	0.04167	0.2730	0.000170	1.93712E-06
	7	Si-7L Si–7V Si-7R	Not Ads.	6	0.04167	0.2730	–	–
Si–C (1.843)	68	Si–C_S86	Ads.	12	0.08333	0.1564	0.682250	0.008891
	78	Si–C_S87	Not Ads.	6	0.04167	0.1564	–	–
	79	Si–C_S97	Ads.	12	0.08333	0.1564	0.000335	4.36673E-06
	69	Si–C_S96	Ads.	6	0.04167	0.1564	0.000386	2.51614E-06
Si–C (1.834)	68	Si–C_S86	Ads.	12	0.08333	0.1564	0.086933	0.001133
	78	Si–C_S87	Not Ads.	6	0.04167	0.1564	–	–
	79	Si–C_S97	Ads.	12	0.08333	0.1564	2.25848E-06	2.94344E-08
	69	Si–C_S96	Ads.	6	0.04167	0.1564	0.000236	1.54067E-06
C–C	86	C–C_S86	Ads.	12	0.08333	0.1355	0.003599	4.06322E-05
	87	C–C_S87	Ads.	6	0.04167	0.1355	0.000901	5.08619E-06
	97	C–C_S97	Ads.	12	0.08333	0.1355	0.000506	5.71169E-06
	96	C–C_S96	Ads.	6	0.04167	0.1355	0.010902	6.15568E-05
							Sticking Coefficient	0.012261

polarity and the adsorbent ($4H-SiC(000\bar{1})_C$ π-bonded chain (π-BC)), as shown in Fig. 3 (a), (f), and (g). There are two (2) sites on the adsorbate, with C-site being the most electronegative (reactive). Whilst on the surface of the hexagonal π-bonded chain (π-BC) lies four atom sites (9, 6, 8, and 7), four bond sites (1, 2, 3, and 4 corresponding to 7–9, 6–9, 6–8 and 7–8 bond respectively). The bond notation for the adsorption is based on, when the silicon atom is first bonded to the surface carbon atom (i.e. forming Si–C). The existence of a hollow site, (5), in the middle of the hexagonal layer, makes it nine surface active sites in total.

Adsorption is examined by first determining the minimum adsorption distance of 1.936 Å for SiC gas on the $4H-SiC(000\bar{1})_C$ π-bonded chain (π-BC) surface. Thereafter, three adsorbate orientations of vertical, 45-degree left and right for on top surface atom positions were considered (9, 6, 8, and 7, pending on whether Si or C adsorbate are to be adsorbed on the surface sites to form SiC). Four possible orientations for the bond sites exist, that is, horizontal bondage of the adsorbate with the surface bond sites (1, 2, 3, and 4). Since the carbon of the SiC adsorbate is more reactive, SiC to surface reactivity could be more when the carbon of the adsorbate is adsorbed on the surface carbon atom than the neighboring silicon atom. For this reason, we adsorbed the carbon of the adsorbate in the vertical, 45-degree left and right orientation on surface atom seven (7), and provide optimized structures of the models in Fig. S1 (q), (r), and (s). Results of the optimized structures and energies, for all the possible sites of the SiC adsorbed on the π-bonded chain (π-BC)

Table 6
Adsorption sites, status, number of surface binding sites and sticking coefficient of $Si_2C_{2(g)}$ at 2186 K.

Atom/Bond Site	Surface Site	Site	Adsorption Status	No. of Binding Site	Probability (P_s)	Fraction of Area (f_A)	Boltzmann Term (β_P)	Site Sticking Coefficient (S_c)
1	6	Si-6L						
		Si–6V	Ads.	6	0.0263	0.2730	0.000209	1.49989E-06
		Si-6R						
	7	Si-7L	Not Ads.	6	0.0263	0.2730	–	–
		Si–7V						
		Si-7R						
2	8	C-8L	Ads.	6	0.0263	0.2372	0.020145	0.000126
		C–8V						
		C-8R						
	9	C–9V	Not Ads.	6	0.0263	0.2372	–	–
1	6	Si-6L						
		Si–6V	Ads.	6	0.0263	0.2730	0.000209	1.49989E-06
		Si-6R						
	7	Si-7L	Not Ads.	6	0.0263	0.2730	–	–
		Si–7V						
		Si-7R						
Si–C	68	Si–C_S86	Ads.	12	0.0526	0.1564	0.220653	0.001816
	78	Si–C_S87	Ads.	6	0.0263	0.1564	1.65919E-05	6.82999E-08
	79	Si–C_S97	Ads.	12	0.0526	0.1564	5.73698E-07	4.72230E-09
	69	Si–C_S96	Not Ads.	6	0.0263	0.1564	–	–
C–C	86	C–C_S86	Ads.	12	0.0526	0.1355	0.076519	0.000546
	87	C–C_S87	Not Ads.	6	0.0263	0.1355	–	–
	97	C–C_S97	Ads.	12	0.0526	0.1355	9.30996E-05	6.63927E-07
	96	C–C_S96	Not Ads.	6	0.0263	0.1355	–	–
2	8	C-8L	Ads.	6	0.0263	0.2372	0.020145	0.000126
		C–8V						
		C-8R						
	9	C–9V	Not Ads.	6	0.0263	0.2372	–	–
Si–C	68	Si–C_S86	Ads.	12	0.0526	0.1564	0.220653	0.001816
	78	Si–C_S87	Ads.	6	0.0263	0.1564	1.65919E-05	6.82999E-08
	79	Si–C_S97	Ads.	12	0.0526	0.1564	5.73698E-07	4.72230E-09
	69	Si–C_S96	Not Ads.	6	0.0263	0.1564	–	–
Si–C	68	Si–C_S86	Ads.	12	0.0526	0.1564	0.220653	0.001816
	78	Si–C_S87	Ads.	6	0.0263	0.1564	1.65919E-05	6.82999E-08
	79	Si–C_S97	Ads.	12	0.0526	0.1564	5.73698E-07	4.72230E-09
	69	Si–C_S96	Not Ads.	6	0.0263	0.1564	–	–
Si–C	68	Si–C_S86	Ads.	12	0.0526	0.1564	0.220653	0.001816
	78	Si–C_S87	Ads.	6	0.0263	0.1564	1.65919E-05	6.82999E-08
	79	Si–C_S97	Ads.	12	0.0526	0.1564	5.73698E-07	4.72230E-09
	69	Si–C_S96	Not Ads.	6	0.0263	0.1564	–	–
							Sticking Coefficient	0.008066

model, are provided explicitly in Fig. S1 (a)–(s) and Table S1 of the supplementary data, respectively. Our finding shows that carbon of the adsorbate, adsorbed on surface carbon site seven (7), 45-degrees right while neighboring silicon atom (T7C_R) is the most feasible of SiC gas on $4H-SiC(000\overline{1})_C$ π-bonded chain (π-BC) surface adsorption.

3.3. $SiC_{2(g)}$ *Species adsorption*

As reported in Ref. [13] investigation of SiC gas-phase reactions, $SiC_{2(g)}$ dominance at equilibrium in the PVT process arises from the sublimation reactions rather than from the lateral interaction reactions. This specie's dominance gives a glimpse of insight into its contribution to the SiC growth rate since dominance literally translates to an increase in deposition rate. In light of the above, we, therefore, considered molecular $SiC_{2(g)}$ adsorption on the reconstructed $4H-SiC(000\overline{1})_C$ π-bonded chain (π-BC) surface, by first identifying the number of sites in the molecule, considering its asymmetry and polarity. The resulting site numbers were three atom sites and two bond sites, and the veracity of its asymmetry can be ascertained from its bond lengths, shown in Fig. 3 (b). Bearing in mind the substrate surface sites are known, as depicted in Fig. 3 (f) and (g).

Carbon atoms 1 and 2 are adsorbed on silicon surface atoms 8 and 9, in vertical, 45-degrees left, and 45-degrees right orientations. Likewise, silicon atom 3 is adsorbed on carbon surface atoms 6 and 7, in the same manner as the aforementioned description. In situations where the molecule is to be adsorbed in the groove, an inclination of 45° either left or right might result in electron cloud repulsion due to the closeness of the adsorbate to the adsorbent groove. For such cases, the model is discarded, as it is unrealistic and not feasible. The three bond sites of Si–C (1.834 Å), Si–C (1.843 Å), and C–C (1.285 Å) are each adsorbed on the four surface bridge sites whilst still maintaining the adsorption distance of 1.850 Å. These combinations are carried out this way, in order to exhaust all the possibilities of finding the surface binding sites for surface adsorption. Fig. S2 and Table S2 in the supplementary data, provide the equilibrium geometries of all the possible combinations for molecular to surface atom sites and molecular bond sites to surface bond sites and a tabular presentation of every site with its corresponding energies. From the given table, the Si–C (1.843 Å) site, on surface sites 6–8, with a bond length of 1.791 Å, is the surface binding site for $SiC_{2(g)}$ adsorption, with adsorption energy of −2.7796 eV.

3.4. $Si_2C_{2(g)}(I_1)$ *Species adsorption*

Adsorption of $Si_2C_{2(g)}(I_1)$ species on the reconstructed $4H-SiC(000\overline{1})_C$ π-bonded chain (π-BC) surface is considered in this silicon carbide crystal growth investigation, due to the fact that, at reduced temperature (2186 K) [13] around the seed layer, the nucleation and evolution of $Si_2C_{2(g)}(I_1)$ species is much rapid and faster than those of $SiC_{2(g)}$, $Si_2C_{(g)}$, $Si_3C_{3(g)}(I_1\ \&\ I_2)$ and $SiC_{(g)}$ species, respectively. Its nucleation and evolution are due to under-cooling, for which temperature serves as a driving force for its species to nucleate and grow on the

Table 7
Adsorption sites, status, number of surface binding sites and sticking coefficient of $Si_4C_{2(g)}(I_1)$ at 2186 K.

Atom/Bond Site	Surface Site	Site	Adsorption Status	No. of Binding Site	Probability (P_s)	Fraction of Area (f_A)	Boltzmann Term (β_P)	Site Sticking Coefficient (S_c)
C1	8	C1–8V						
		C1-8R	Not ads.	6	0.01190	0.2372	–	–
		C1-8VR						
	9	C1–9V	Not ads.	6	0.01190	0.2372	–	–
C2	8	C2–8V						
		C2-8R	Not ads.	6	0.01190	0.2372	–	–
		C2-8VR						
	9	C2–9V	Not ads.	6	0.01190	0.2372	–	–
3	6	Si3-6L	Ads.	6	0.01190	0.2730	0.684828	0.002225
		Si3–6V						
		Si3-6R						
	7	Si3–7V	Not ads.	6	0.01190	0.2730	–	–
4	6	Si4-6L						
		Si4–6V	Ads.	6	0.01190	0.2730	0.110046	0.000358
		Si4-6R						
	7	Si4-7L						
		Si4–7V	Not ads.	6	0.01190	0.2730	–	–
		Si4-7R						
5	6	Si5-6L						
		Si5–6V	Not ads.	6	0.01190	0.2730	–	–
		Si5-6R						
	7	Si5-7L						
		Si5–7V	Not ads.	6	0.01190	0.2730	–	–
		Si5-7R						
6	6	Si6-6L						
		Si6–6V	Not ads.	6	0.01190	0.2730	–	–
		Si6-6R						
	7	Si6–7V	Not ads.	6	0.01190	0.2730	–	–
Si–C (1.835)	68	Si–C_S68	Ads.	12	0.02381	0.1564	0.000349	1.30053E-06
	78	Si–C_S78	Not ads.	6	0.01190	0.1564	–	–
	79	Si–C_S79	Not ads.	12	0.02381	0.1564	–	–
	69	Si–C_S69	Not ads.	6	0.01190	0.1564	–	–
Si–Si (2.453)	68	Si–Si_S68	Not ads.	12	0.02381	0.1533	–	–
	78	Si–Si_S78	Not ads.	6	0.01190	0.1533	–	–
	79	Si–Si_S79	Not ads.	12	0.02381	0.1533	–	–
	69	Si–Si_S96	Not ads.	6	0.01190	0.1533	–	–
Si–Si (2.455)	68	Si–Si_S68	Not ads.	12	0.02381	0.1533	–	–
	78	Si–Si_S78	Not ads.	6	0.01190	0.1533	–	–
	79	Si–Si_S79	Not ads.	12	0.02381	0.1533	–	–
	69	Si–Si_S96	Not ads.	6	0.01190	0.1533	–	–
C–C	86	C–C_S68	Ads.	12	0.02381	0.1355	0.000172	5.54091E-07
	87	C–C_S87	Not ads.	6	0.01190	0.1355	–	–
	97	C–C_S97	Not ads.	12	0.02381	0.1355	–	–
	96	C–C_S96	Not ads.	6	0.01190	0.1355	–	–
Si–Si (2.453)	68	Si–Si_S68	Not ads.	12	0.02381	0.1533	–	–
	78	Si–Si_S78	Not ads.	6	0.01190	0.1533	–	–
	79	Si–Si_S79	Not ads.	12	0.02381	0.1533	–	–
	69	Si–Si_S96	Not ads.	6	0.01190	0.1533	–	–
Si–C (1.834)	68	Si–C_S68	Ads.	12	0.02381	0.1564	0.000635	2.36313E-06
	78	Si–C_S78	Not ads.	6	0.01190	0.1564	–	–
	79	Si–C_S79	Not ads.	12	0.02381	0.1564	–	–
	69	Si–C_S69	Not ads.	6	0.01190	0.1564	–	–
Si–C (2.129)	68	Si–C_S68	Ads.	12	0.02381	0.1564	0.032717	0.000122
	78	Si–C_S78	Not ads.	6	0.01190	0.1564	–	–
	79	Si–C_S79	Not ads.	12	0.02381	0.1564	–	–
	69	Si–C_S69	Not ads.	6	0.01190	0.1564	–	–
Si–C (2.129)	68	Si–C_S68	Ads.	12	0.02381	0.1564	0.032717	0.000122
	78	Si–C_S78	Not ads.	6	0.01190	0.1564	–	–
	79	Si–C_S79	Not ads.	12	0.02381	0.1564	–	–
	69	Si–C_S69	Not ads.	6	0.01190	0.1564	–	–
Si–Si (2.451)	68	Si–Si_S68	Not ads.	12	0.02381	0.1533	–	–
	78	Si–Si_S78	Not ads.	6	0.01190	0.1533	–	–
	79	Si–Si_S79	Not ads.	12	0.02381	0.1533	–	–
	69	Si–Si_S96	Not ads.	6	0.01190	0.1533	–	–
Si–Si (2.452)	68	Si–Si_S68	Not ads.	12	0.02381	0.1533	–	–
	78	Si–Si_S78	Not ads.	6	0.01190	0.1533	–	–
	79	Si–Si_S79	Not ads.	12	0.02381	0.1533	–	–
	69	Si–Si_S96	Not ads.	6	0.01190	0.1533	–	–
Si–C (2.130)	68	Si–C_S68	Ads.	12	0.02381	0.1564	0.057310	0.000213
	78	Si–C_S78	Not ads.	6	0.01190	0.1564	–	–
	79	Si–C_S79	Not ads.	12	0.02381	0.1564	–	–
	69′	Si–C_S69	Not ads.	6	0.01190	0.1564	–	–
Si–C (2.131)	68	Si–C_S68	Ads.	12	0.02381	0.1564	0.081227	0.000302

(*continued on next page*)

Table 7 (*continued*)

Atom/Bond Site	Surface Site	Site	Adsorption Status	No. of Binding Site	Probability (P_s)	Fraction of Area (f_A)	Boltzmann Term (β_P)	Site Sticking Coefficient (S_c)
	78	Si–C_S78	Not ads.	6	0.01190	0.1564	–	–
	79	Si–C_S79	Not ads.	12	0.02381	0.1564	–	–
	69′	Si–C_S69	Not ads.	6	0.01190	0.1564	–	–
							Sticking Coefficient	0.003346

substrate, as evident from the Kinetic Monte Carlo simulation and classical approach in Ref. [13]. In order to accurately predict its surface binding site, taking into account the number of surface sites that have previously been found (see Fig. 3 (f) and (g)), an analysis on the $Si_2C_{2(g)}(I_1)$ molecule was then carried out, for which symmetry was first identified due to the equality in Si–C bond length (Fig. 3 (c)). The symmetry line shown in a long dash red color shows one-half of the molecule is a mirror image of the other half. Taking into account the aforementioned, two atomic sites of silicon and carbon, and two molecular bond sites of Si–C and C–C bonds are pinpointed for calculation, and the other symmetric half taking into account for further analysis as shown in the Tables.

In order to find the surface binding site, adsorption of the identified atomic sites were first carried out, by adsorbing molecular silicon and carbon sites on surface atom sites of carbon (6 and 7) and silicon (8 and 9) atoms, respectively, in orientations of vertical, 45-degrees left and 45-degrees right. In cases where inclined adsorption (45-degree left or right) of the molecule is not feasible, such as molecular carbon site adsorption on groove surface silicon (Si 9) of the π-bonded chain (π-BC) surface, only vertical adsorption of the molecule is realistic (Fig. S3 (j)), and should be considered as practical. Molecular bond sites of Si–C and C–C are each adsorb separately, on the four surface bond sites (6–8, 7–8, 7–9, and 6–9) of the π-bonded chain (π-BC) surface. For clarity, this convention is chosen for bond sites in such a way that, when silicon from the molecular side is bonded with the surface carbon atom (to form a Si–C bond), the surface carbon atom number precedes the next surface atom (silicon) making a bond with another molecular atom. Equilibrium geometries of all the site combinations are shown in Fig. S3 of the supplementary, for visual observation. An explicit analysis of their energies presented in Table S3 shows the Si–C bond site of the molecule is the preferred surface binding site on surface 8-6 of the π-bonded chain (π-BC) surface, which record adsorption energy of −2.4562 eV among others. This result is another confirmation that the surface binding site is Si–C bond 6–8.

3.5. $\mathbf{Si_4C_{2(g)}(I_1)}$ *Species adsorption*

Evidence from previous Kinetic Monte Carlo (KMC) investigation of silicon carbide PVT gas-phase reactions, shows isomers of tetra silicon dicarbide $Si_4C_{2(g)}$ (I_1 & I_2) as the most copious species among others, present in the PVT system [13], due to the kinetics of their resulting reaction involving a high influx of silicon. Thus, these clusters should be considered as some of the most important growth contributing silicon carbide species, counting on their abundance, which literally translates to an increase in impingement rate. Equilibrium geometry of $Si_4C_{2(g)}(I_1)$ [13] obtained from Gaussian 03 software optimization, shows good agreement of equilibrium energy and bond lengths with previous ab-initio calculations [42]. Each of the bond lengths as observed, is exclusively different from the rest, implying asymmetry of the molecule. This led to the identification of six atomic sites and twelve bond sites of the molecule, of which five of the bonds are Si–Si, six are of Si–C bond types and one is C–C bond.

For the adsorption of $Si_4C_{2(g)}(I_1)$ species on the π-bonded chain (π-BC) surface, we maintained the previous approach, by adsorbing silicon atoms of the molecule (3, 4, 5, and 6) on surface carbon atoms (6 and 7), in vertical orientations, 45-degree left, and 45-degree right. Likewise, for the carbon atom of the adsorbate, carbon atoms (1 and 2) are adsorbed on the surface silicon atoms (8 and 9) of the π-bonded chain (π-BC), in the same aforementioned orientations. It should be noted that, in cases where a molecule is to be adsorbed in the groove, 45-degree left or right orientations are not feasible nor practical, as the molecule gets shattered (Fig. S4 (p), (r), (v), (x)) due to high electronic repulsion of the electron cloud. Hence, only vertical orientation is a reasonable geometry orientation. As for the bond sites, Si–Si, C–C, and Si–C molecular bond sites are adsorbed on the four available surface bond sites (6–8, 7–8, 7–9, and 6–9) of the π-bonded chain (π-BC) surface. All the molecular bond sites were adsorbed on these surface sites for binding site search, except Si–C bond sites 1.834, 2.129, 2.130, and 2.131 Å which were only adsorbed on surface site 6–8, due to the fact that prior adsorption calculations of $Si_2C_{2(g)}(I_1)$, $SiC_{2(g)}$ and $Si_4C_{2(g)}(I_2)$ (see below section) reveals 6–8 as the surface binding site. As compared to other molecules, where the molecular binding site is the Si–C bond, $Si_4C_{2(g)}(I_1)$ case is somewhat different, as the C–C bond site is more reactive than other bonds.

3.6. $\mathbf{Si_4C_{2(g)}(I_2)}$ *Species adsorption*

$Si_4C_{2(g)}(I_2)$ is considered as the second most abundant silicon carbide growth contributing species. Therefore, we utilized its optimized geometry for surface binding site investigation on the reconstructed 4H − $SiC(000\bar{1})_C$ π-bonded chain (π-BC) surface. Equilibrium bond lengths of the optimized molecule agreed with those reported in Ref. [43], and the molecule is asymmetry. This implies that each atom site, as well as bond sites, will exhibit unique adsorption energy and must be labeled and investigated on the surface separately, in order to find the molecular and surface binding site. We, therefore, identified six different atom sites, for which two are carbon atom sites, four are silicon atom sites, and ten bond sites, which include six Si–C bonds, three Si–Si bonds, and a single C–C bond site as shown picturesque in Fig. 3(e).

Each atom site is adsorbed in 45-degree left, right and vertical orientation via density functional theory (DFT) simulation on either of the two surface atom sites 9 (Si), 6 (C), 8 (Si), and 7 (C), depending on which molecular atom site is to be adsorbed. Likewise, for the bond sites, Si–C bonds, Si–Si bonds, and C–C bonds are adsorbed on surface bridge sites 6–8, 7–8, 9–7, and 6–9 for each bond investigation. The DFT analysis reveals that the Si–C molecular bond site of bond length 1.851 Å is the binding site on surface site 6–8. Explicit values of the adsorption energies for each molecule, their corresponding surface binding sites, molecular active site's bond lengths, system minimum energy, and molecule-to-surface minimum adsorption distance are tabulated in Table II.

3.7. *Sticking coefficient*

In order to estimate the sticking coefficient of individual species on the substrate, we first investigate for dissociative adsorption and found out that, clusters/molecules of $Si_2C_{2(g)}(I_1)$, $SiC_{2(g)}$, $Si_4C_{2(g)}(I_1)$ and $Si_4C_{2(g)}(I_2)$ do not actually dissociate on the surface to form $2SiC_{(g)}$, $SiC_{(g)} + C_{(g)}$ and $2Si_2C_{(g)}$ (for $Si_4C_{2(g)}(I_1\&I_2)$), respectively, but rather, they are adsorbed as clusters/molecules on the substrate to form solid silicon carbide ($SiC_{(c)}$). This conclusion is ascertained via the adsorption of 2 mol of silicon carbide ($2SiC_{(g)}$) on the Si–C_S86 site and its neighboring site (see Fig. 4(a–d)), and also, on $SiC_{(g)}$ site (T7C_R) and its

Table 8
Adsorption sites, status, number of surface binding sites, and sticking coefficient of $Si_4C_{2(g)}(I_2)$ at 2186 K.

Atom/Bond Site	Surface Site	Site	Adsorption Status	No. of Binding Site	Probability (P_s)	Fraction of Area (f_A)	Boltzmann Term (β_P)	Site Sticking Coefficient (S_c)
1	6	Si1-6L	Ads.	6	0.01389	0.2730	2.88781E-05	1.09505E-07
		Si1–6V						
		Si1-6R						
	7	Si1-7L						
		Si1–7V	Not Ads.	6	0.01389	0.2730	–	–
		Si1-7R						
2	8	C2-8L						
		C2–8V	Ads.	6	0.01389	0.2372	5.64912E-05	1.86122E-07
		C2-8R						
	9	C2–9V	Ads.	6	0.01389	0.2372	1.65735E-05	5.46050E-08
3	6	Si3-6L						
		Si3–6V	Ads.	6	0.01389	0.2730	0.001052	3.98965E-06
		Si3-6R						
	7	Si3-7L	Not Ads.	6	0.01389	0.2730	–	–
		Si3–7V						
		Si3-7R						
4	8	C4-8L						
		C4–8V	Ads.	6	0.01389	0.2372	0.011999	3.95321E-05
		C4-8R						
	9	C4–9V	Ads.	6	0.01389	0.2372	0.000370	1.21946E-06
5	6	Si5-6L						
		Si5–6V	Ads.	6	0.01389	0.2730	0.000181	6.88003E-07
		Si5-6R						
	7	Si5–7V	Not ads.	6	0.01389	0.2730	–	–
6	6	Si6-6L						
		Si6–6V						
		Si6-6R	Ads.	6	0.01389	0.2730	8.75353E-05	3.31931E-07
	7	Si6-7L						
		Si6–7V	Not Ads.	6	0.01389	0.2730	–	–
		Si6-7R						
Si–Si (2.481)	68	Si–Si_S68	Not Ads.	12	0.02778	0.1533	–	–
	78	Si–Si_S78	Not Ads.	6	0.01389	0.1533	–	–
	97	Si–Si_S97	Not Ads.	12	0.02778	0.1533	–	–
	69	Si–Si_S69	Not Ads.	6	0.01389	0.1533	–	–
Si–Si (2.479)	68	Si–Si_S68	Not Ads.	12	0.02778	0.1533	–	–
	78	Si–Si_S78	Not Ads.	6	0.01389	0.1533	–	–
	97	Si–Si_S97	Not Ads.	12	0.02778	0.1533	–	–
	69	Si–Si_S69	Not Ads.	6	0.01389	0.1533	–	–
	68	Si–Si_S68	Not Ads.	12	0.02778	0.1533	–	–
	78	Si–Si_S78	Not Ads.	6	0.01389	0.1533	–	–
Si–Si (2.478)	97	Si–Si_S97	Not Ads.	12	0.02778	0.1533	–	–
	69	Si–Si_S69	Not Ads.	6	0.01389	0.1533	–	–
	68	Si–C_S68	Ads.	12	0.02778	0.1564	0.018991	8.25137E-05
	78	Si–C_S78	Ads.	6	0.01389	0.1564	2.46658E-05	5.35839E-08
Si–C (1.788)	97	Si–C_S97	Ads.	12	0.02778	0.1564	0.002172	9.43490E-06
	69	Si–C_S96	Not Ads.	6	0.01389	0.1564	–	–
	68	Si–C_S68	Ads.	12	0.02778	0.1564	0.000482	2.09476E-06
	78	Si–C_S78	Not Ads.	6	0.01389	0.1564	–	–
Si–C (2.058)	97	Si–C_S97	Not Ads.	12	0.02778	0.1564	–	–
	69	Si–C_S96	Ads.	6	0.01389	0.1564	1.76168E-05	3.82708E-08
	68	Si–C_S68	Ads.	12	0.02778	0.1564	0.010216	4.43860E-05
	78	Si–C_S78	Ads.	6	0.01389	0.1564	2.42761E-05	5.27373E-08
Si–C (1.832)	97	Si–C_S97	Not Ads.	12	0.02778	0.1564	–	–
	69	Si–C_S96	Not Ads.	6	0.01389	0.1564	–	–
	68	Si–C_S68	Ads.	12	0.02778	0.1564	2.82864E-05	1.22898E-07
	78	Si–C_S78	Not Ads.	6	0.01389	0.1564	–	–
Si–C (2.083)	97	Si–C_S97	Not Ads.	12	0.02778	0.1564	–	–
	69	Si–C_S96	Ads.	6	0.01389	0.1564	1.48094E-05	3.2172E-08
	68	Si–C_S68	Ads.	12	0.02778	0.1564	0.941905	0.004092
	78	Si–C_S78	Not Ads.	6	0.01389	0.1564	–	–
Si–C (1.851)	97	Si–C_S97	Ads.	12	0.02778	0.1564	0.001500	6.51696E-06
	69	Si–C_S96	Ads.	6	0.01389	0.1564	3.5127E-05	7.63097E-08
	68	Si–C_S68	Ads.	12	0.02778	0.1564	0.008062	3.50285E-05
	78	Si–C_S78	Ads.	6	0.01389	0.1564	0.000159	3.45716E-07
Si–C (1.985)	97	Si–C_S97	Not Ads.	12	0.02778	0.1564	–	–
	69	Si–C_S96	Not Ads.	6	0.01389	0.1564	–	–
	68	C–C_S68	Not Ads.	12	0.02778	0.1355	–	–
	87	C–C_S87	Ads.	6	0.01389	0.1355	0.000170	3.19897E-07
C–C (1.516)	97	C–C_S97	Ads.	12	0.02778	0.1355	0.002406	9.05598E-06
	69	C–C_S96	Not Ads.	6	0.01389	0.1355	–	–
							Sticking Coefficient	0.004329

Table 9
Adsorption sites, status, number of surface binding sites and sticking coefficient of $Si_2C_{(g)}$ at 2186 K.

Atom/Bond Site	Surface Site	Site	Adsorption Status	No. of Binding Site	Probability (P_s)	Fraction of Area (f_A)	Boltzmann Term (β_P)	Site Sticking Coefficient (S_c)
1	8	C-8L C–8V C-8R	Ads.	6	0.04167	0.2372	0.078453	0.000775
	9	C-9L C–9V	Ads.	6	0.04167	0.2372	0.000286	2.82216E-06
2	6	Si-6L Si–6V Si-6R	Ads.	6	0.04167	0.2730	4.25499E-05	4.84044E-07
	7	Si-7L Si–7V Si-7R	Ads.	6	0.04167	0.2730	4.30269E-05	4.89471E-07
2	6	Si-6L Si–6V Si-6R	Ads.	6	0.04167	0.2730	0.454942	0.005929
	7	Si-7L Si–7V Si-7R	Ads.	6	0.04167	0.2730	7.66614E-05	4.99617E-07
Si–C	68	SiC_S68	Ads.	12	0.08333	0.1564	0.005400	3.51949E-05
	87	SiC_S87	Ads.	6	0.04167	0.1564	0.000251	3.20771E-06
	97	SiC_S97	Not Ads.	12	0.08333	0.1564	–	–
	96	SiC_S96	Ads.	6	0.04167	0.1564	0.454942	0.005929
Si–Si	68	SiSi_S68	Ads.	12	0.08333	0.1533	7.66614E-05	4.99617E-07
	87	SiSi_S87	Not Ads.	6	0.04167	0.1533	–	–
	97	SiSi_S97	Not Ads.	12	0.08333	0.1533	–	–
	96	SiSi_S96	Not Ads.	6	0.04167	0.1533	–	–
Si–C	68	SiC_S68	Ads.	12	0.08333	0.1564	0.005400	3.51949E-05
	87	SiC_S87	Ads.	6	0.04167	0.1564	4.25499E-05	4.84044E-07
	97	SiC_S97	Not Ads.	12	0.08333	0.1564	–	–
	96	SiC_S96	Ads.	6	0.04167	0.1564	4.30269E-05	4.89471E-07
							Sticking Coefficient	0.012713

Table 10
Adsorption sites, status, number of surface binding sites and sticking coefficient of $Si_{(g)}$ at 2186 K.

Atom Site	Surface Site	Site	Adsorption Status	No. of Binding Site	Probability (P_s)	Fraction of Area (f_A)	Boltzmann Term (β_P)	Site Sticking Coefficient (S_c)
Si	6	T1_6	Ads.	6	0.10526	0.2730	0.977721	0.028096
	7	T2_7	Ads.	6	0.10526	0.2730	0.009669	0.000278
	5	Hollow	Not Ads.	9	0.15789	–	–	–
Si	96	Si_S96	Not Ads.	6	0.10526	–	–	–
	68	Si_S68	Not Ads.	12	0.21053	–	–	–
	87	Si_S87	Ads.	6	0.10526	0.2730	0.009855	0.000283
	97	Si_S97	Ads.	12	0.21053	0.2730	0.002755	0.000158
							Sticking Coefficient	0.028815

Table 11
Comparison of silicon carbide (PVT) experimental growth rate with simulation.

Current work/Benchmarking Literatures	Seed temperature (K)	Growth pressure (mbar)	Source to seed distance (mm)	Axial temperature gradient K/cm	Growth rate (mm/h)	Crystal type	Method
This work	2529	1.33	82	2.2–3.4	0.62	4H	Simulation
		3.99			0.50		
		6.66			0.41		
		13.33			0.28		
		26.66			0.18		
Selder, M. et al. [60]	2498–2512			25	0.18–0.24		Simulation
Tymicki, E. et al. [61]	2573	100–300	30	26.67	0.11–0.16	6H	Experiment
Tupitsyn, E. Y. et al. [62]	2223–2523	13.3–39.9	50		1–1.12	4H/6H	Experiment
Chen, Q. S. et al. [63]	2671	80–120			0.45–0.85		Simulation
Barrett, D. L. et al. [64]	≈2140	0.27	5–47	100	0.75	6H	Experiment
	≈2453	2.66			1.1–1.2		
	≈2513	6.65			1.2		
	≈2533	26.6			0.3–0.6		

neighboring site to form $2SiC_{(g)}$ on the substrate. The former configuration forms a linear isomer of $Si_2C_{2(g)}$ on the surface, which conforms with the $4H-SiC(000\bar{1})_C$ growth behavior, but appears to be of higher energy than adsorb $Si_2C_{2(g)}(I_1)$. This implies that $Si_2C_{2(g)}(I_1)$ cluster adsorption on the substrate is the adsorb/right configuration. The latter configuration of $2SiC_{(g)}$ (T7C_R and its neighboring site) has much lower energy than the former, but higher energy than adsorbing $Si_2C_{2(g)}(I_1)$

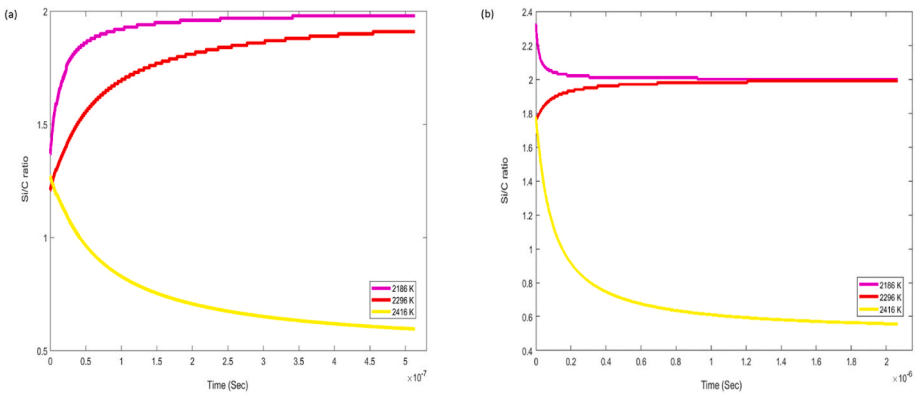

Fig. 6. Estimated Si/C ratio with time, on the reconstructed 4H − $SiC(000\bar{1})_C$ π-bonded chain (π-BC) substrate. (a) Without coupling the Boltzmann term (b) When the Boltzmann term is coupled.

cluster. Similar investigation for $SiC_{2(g)}$, $Si_4C_{2(g)}(I_1)$ and $Si_4C_{2(g)}(I_2)$ is also carried out on the reconstructed 4H − $SiC(000\bar{1})_C$ π-bonded chain (π-BC) surface and the conclusion remains the same.

For the sticking coefficient estimation of each molecule, we utilize the system energy of each adsorption site, and calculate the adsorption energies of the sites (see Tables S1–S5 in the supplementary information), in order to know the status of adsorption on each specific site. Furthermore, the probability of the site is calculated via counting for each site, the number of identical sites on the substrate, and the ratio of the identical sites to the total number of sites is taken as the probability of sites. From equation (2) in the prior section, the sticking coefficient of an individual site is derived as the product of its probability, fractional area and Boltzmann probability term (when the term is coupled). The fractional area as defined is the ratio of the sticking surface (bond circular point of contact) to the atom/bond surface area. To have a better understanding, we respectively provide models of bond surface area for Si–C, Si–Si, and C–C; both conventional bond models (Fig. 5 (a), (b) and (c)) and hard-sphere (Fig. 5 (d), (e) and (f)), and atomic site sticking model (Fig. 5 (g)).

In the case of atomic site sticking (silicon or carbon), the tip of the bond formed (be it silicon or carbon bond) is considered as the sticking surface, which is calculated by using the molecular single bond covalent radius provided in Table III, and the atomic surface area using the covalent radius. Likewise, for the bond-site sticking, we made use of the same approach, by calculating the sticking surface area for the two bonds formed. Here, the molecular single bond covalent radius will be used depending on the types of atoms (or bond) sticking on the surface. For instance, a Si and C, Si and Si, and C and C, molecular single bond covalent radius should be made use of, for Si–C, Si–Si, and C–C bond sticking surface calculation, respectively. Thereafter, the molecular bond shape is also of paramount importance for the accurate prediction of the sticking surface fractional area. This is determined by considering the types of molecular atoms or molecular atoms covalent radii used in molecule bond formation. In a case where the molecular atoms' covalent radii are of the same magnitude (Si–Si and C–C), the bond shape is considered cylindrical, and its surface area, S_{cylind} (see Eqn. (3)) is calculated using the conventional bond model approach or hard-sphere model. However, where the molecular atoms are dissimilar, and whose covalent radii are of different magnitudes (Si–C), the bond shape is considered a frustum, and its area is calculated via the method of similarity in enlargement (Eqn. (4)), in order to first determine the frustum height, for both conventional and hard-sphere models. Afterward, the frustum surface area (S_{frust}) for both models is estimated (see Eqn. (5)).

$$S_{cylind} = 2\pi r^2 + 2\pi rh \tag{3}$$

$$\frac{H}{h} = \frac{d_1}{d_2} \tag{4}$$

$$S_{frust} = \pi(r+R)S' + \pi r^2 + \pi R^2 \tag{5}$$

Where d_1 and d_2 are respectively, diameters of the large and small atoms, H and h are the heights of the extended cone and frustum, respectively. For the surface area, r is the radius of the small atom, R is the radius of the large atom, and S' is the frustum slant height.

In the hard-sphere models, the summation of the two atoms' covalent radii for a specific molecular bond type, gives the bond length. Whereas, the height of the cylindrical (or frustum) shape of the bond, is calculated by summing the other two halves of the covalent radii, of the atoms. In contrast, conventional bond heights are estimated via summation of equilibrium bond length, be it Si-Si [44,45], Si–C [46], or C–C [47] bond, and the diameter of the two atoms. It is apparent, from the provided figures (Fig. 5) and tables (Tables IV–X), that a specific molecular bond type (Si–Si, Si–C, or C–C) is not unique or is dissimilar in length to other bonds of the same type, on the same molecule. Nonetheless, the argument is that bond lengths of the same type, with different lengths on the same molecule, will converge to the equilibrium length (2.358 for Si–Si, 1.749 for Si–C, and 1.54 for C–C) during adsorption. Thus, the use of equilibrium lengths for Si–Si, Si–C, and C–C bonds in all the molecules during the calculation. Thereafter, the fractional surface of the sticking atom or an adsorb bond is calculated, and the sticking coefficient estimation for each molecule, is calculated by computing the sticking coefficient for each site, and having their summation. Tables IV–VIII, provides. When the Boltzmann probability term of the sites is coupled, the minute constant effect of temperature on the sticking coefficient could be observed. For example, the sticking coefficient of $Si_2C_{(g)}$ at 2186, 2296, and 2416 K are respectively, 0.0127, 0.0127 and 0.0126. For $SiC_{(g)}$, the coefficients are 0.0211, 0.0211 and 0.0211, for $Si_2C_{2(g)}$ are 0.0081, 0.0081 and 0.0080, and for $Si_{(g)}$, 0.0288, 0.0288 and 0.0289 are respectively the values, which validates the claim in the Boltzmann term, as an approximate constant.

Since crystal growth is dynamic, and there are likely to be two or more structural changes on the growing substrate before the final growth termination surface [22], the adsorption energies obtained from the surface of the **4H − SiC**$(000\bar{1})_C$ substrate are not ideal or applicable to subsequent growing surfaces/terminations. Considering the fact that our developed method for deriving the sticking coefficient, defines it as, the product of the probability of sites, fractional area of sticking, and Boltzmann term, only the adsorption energy (and temperature) in the Boltzmann term is a variable due to subsequent growing surface termination (structural changes). Since 4H–SiC is hexagonal, the hexagonality of the surface (Fig. 3 (f) and (g)) is not likely to change, and therefore, the probability of sites remains the same. Likewise, for the fractional sticking area, the sticking atoms (be it silicon or carbon) and sticking bonds (Si–Si, Si–C, or C–C) remains the same (see Table III) as the growing surface changes in composition and termination. For every

stage of the structural change in the growing substrate, Tables III and IV–X can be used as a template to compute the sticking coefficient for a specific termination, depending on the molecule of interest. One only has to compute for the adsorption energies of the molecule of interest on the new termination and compute for the Boltzmann term of individual sites at a specific temperature, then couple it with the remaining two terms of the sticking coefficient (probability of sites and fractional sticking area) for every site and take the overall summation. However, in the case of the PVT process, high temperature and low-pressure environment at the growth's surface ensure the layered growth behavior. Surface adsorption is the limited growth process. Thus the sticking coefficients considered in this study should be able to cover most scenarios.

The dynamism of the silicon carbide growth on the $4\mathbf{H}-\mathbf{SiC}(000\bar{1})_{\mathbf{C}}$ π-bonded chain (π-BC) substrate, could be predicted via reactive molecular dynamics simulation using the atom by atom and molecule by molecule deposition approach. However, there are no available experimental in-situ observations for the growth dynamism and stages of growth for the $4\mathbf{H}-\mathbf{SiC}(000\bar{1})_{\mathbf{C}}$ π-bonded chain (π-BC) substrate to compare with in the literature. Since it is quite difficult to determine the sticking coefficient of molecules experimentally, therefore, in order to validate our results and justify our ab-initio approach, we used our estimated sticking coefficients as initial values for continuous modeling in COMSOL MultiPhysics to predict the PVT growth rate using the lateral interaction reactions reported in the work of A. Abubakar Alao & W. D.-Hsu [13], while using a similar geometry to that which they reported. Their calculated rate constants for the intermediate reactions of the lateral interaction reactions were utilized in predicting the final growth rate, using the Hertz-Knudsen model for crystal growth simulation. To make a bit of comparison, we took into consideration parameters such as seed temperature, growth pressure, source-to-seed distance, and axial temperature gradient, and our predicted growth rate, when compared to the experimental/simulated growth of SiC in the PVT process, shows good agreement as presented in Table XI.

3.8. Si/C ratio

It is worth recalling from the PVT process [13], that lateral interaction reactions occur due to the non-ideal behavior of the sublime species at increased source to substrate distance and reduced temperature. If the source to substrate distance is maintained at a reduced length (below the thermalization distance), in such a way that, sublime molecules only behave ideally and the lateral interaction reactions cease to occur, then there will be high $Si_{(g)}$ flux [13], which will make the Si/C ratio deviate much far from unity. However, if the former configuration is adopted, lateral interaction reactions will occur, and molecules will have sufficient space/time to diffuse and silicon carbide compounds will be formed, which might help in maintaining the stoichiometric (Si/C) ratio close to unity. That is the reason for the study of the kinetics and thermodynamics of the lateral interaction reactions in A. Abubakar Alao and W.-D. Hsu's investigation [13]. Furthermore, in order to calculate the Si/C ratio of silicon carbide boule in this configuration, we included $Si_{(g)}$ and $Si_2C_{(g)}$ (see Fig. 4(e) for geometry) species sticking coefficient aside from the above growth contributing species, so as to balance the stoichiometry and include each contributor. Therefore, we present their sticking coefficient results in Tables IX and X (see Supplementary Information Tables S6 and S7 for their energies). The Si/C ratio of the SiC boule in this configuration is calculated via utilization of the calculated sticking coefficient of individual growth contributing species in Table IV through VIII and their reported concentration [13], which was estimated using the Kinetic Monte Carlo approach. Our calculated Si/C ratio, presented in Fig. 6 (a) and (b), shows a rise in the Si/C ratio on the substrate and growth region with time, when the Boltzmann term is not coupled. This rise in Si/C ratio continues to increase until it reaches a constant Si/C ratio of 2.00, 1.98, and 0.53 at 2186, 2296, and 2416 K (concentration temperature). When the Boltzmann term is coupled (Fig. 6 (b)), the evolution of the Si/C ratio curve with time at 2186 K, curves inward and converges to 2.00 when the time reaches (10^{-6}). The trend for the Si/C ratio evolution with time at 2296 and 2416 K remains the same (when Boltzmann term is not coupled), and the Si/C ratio converges to 1.99 and 0.56, respectively.

With or without the Boltzmann term, the Si/C ratio result converges to the aforementioned. The result moreover, opens a wider horizon to understanding the effect of furnace geometry design (source to substrate distance in this case) and system temperature on the type/kind of quality of crystal that will be grown (deviated Si/C ratio resulting in vacancy/defects in Si or C). For instance, at a reduced source to substrate distance where lateral interaction reactions still occur, molecules have sufficient space/time to diffuse and silicon carbide compounds are formed, and also bearing in mind that some molecules still collide with the crucible wall. Then the stoichiometry of the species (Si/C ratio) will be much closer to unity compared to when placed much farther apart. This implies that, as one reduces the source to substrate distance (alters the geometry configuration), the Si/C ratio converges "towards" unity. The concept of source-to-substrate distance reduction can also be viewed from the perspective of substrate species concentration being proportional to the traveling distance/diffusion time. The concentration of species on the substrate gradually decreases as the source to substrate distance is maintained farther apart.

The temperature effect on the Si/C ratio is another factor to be critical/worried of, as the Si/C ratio is largely dependent on the concentration temperature. It is observed from Fig. 6 (a) and (b) that at reduced temperature, 2186 K, much further from the sublimation temperature of the SiC source, 2700 K [48], the Si/C ratio deviates from unity. Likewise, as the temperature rises to a higher value, 2296 K (mid of the growth chamber), before the optimum value, the Si/C ratio is seen to deviate "away" from unity. At a temperature of 2416 K, immediately above the charged surface/source region, the Si/C ratio decreases with time, converges to unity and beyond (then becomes a constant), and the behavior of the Si/C ratio curve is inverse of the prior mentioned temperatures, and this is justified by the previous works of Ariyawong [49], JANAF [50], Lilov [51], Rocabois [52,53] and SGPS database [54,55]. It is reported from their work, that the Si/C ratio will converge and fall below unity at a temperature of 2400 K and above (temperature around the charge source), as carbon specie's sublimation is sustained more at a higher temperature. It should be borne in mind also, that for high-quality growth of SiC ingot, not only the Si/C ratio affects defect/vacancy concentration but temperature as well. The inversion/switch in the behavior of the curve is due to a stoichiometric ratio change in carbon, as carbon sublimation is sustained at a higher temperature, it dominates silicon (as some silicon becomes liquid), while silicon dominates at reduced temperature.

4. Conclusion

An ab-initio investigation, on the sticking coefficient of silicon carbide growth species on the reconstructed $4H-SiC(000\bar{1})_C$ π-bonded chain (π-BC) substrate and their Si/C ratio in the physical vapor transport (PVT) process have been studied. The C-face of the $4H-SiC(000\bar{1})$ π-bonded chain surface is the most stable substrate among others, and the sticking coefficient of smaller growth species, such as $SiC_{(g)}$, $SiC_{2(g)}$, $Si_{(g)}$ and $Si_2C_{(g)}$ is superior to those of cluster molecules. Si/C ratio in the bulk fluid regime is largely dependent on the concentration temperature and an analysis of the Si/C ratio on the substrate (2186 K) and 2296 K reveals a non-unity stoichiometric ratio of silicon to carbon, which increases over time, to a constant value. It is observed from the results that, at distance below the substrate in the bulk flow regime or temperature correspondence, higher temperature fluid regime, the Si/C ratio tends to approach unity, converge and exceed. This implies that, in order to decrease the defect concentration (missing carbon atoms) in grown silicon carbide boule, the source to substrate distance should be

smaller or shorter than the conventional distance. However, this is not the absolute solution to defect eradication in silicon carbide boule from the PVT system, because the source to substrate distance reduction converges the stoichiometry of Si/C to unity at a higher temperature, and the 4H − SiC substrate cannot be placed at a higher temperature for crystal stability (polytype stability). Therefore, it is recommended that extra carbon sources in the form of graphitized powder be added to the silicon carbide source, and the kinetics and thermodynamics of the whole process be revisited.

CRediT authorship contribution statement

Ahmed Abubakar Alao: Writing – review & editing, Visualization, Validation, Methodology, Investigation, Data curation. **Weng-Ngai Wu:** Data curation. **Wen-Dung Hsu:** Writing – review & editing, Supervision, Methodology, Investigation, Funding acquisition, Conceptualization.

Declaration of competing interest

The authors declare that they have no known competing financial interests or personal relationships that could have appeared to influence the work reported in this paper.

Data availability

Data will be made available on request.

Acknowledgement

This research was financially supported by the Hierarchical Green-Energy Materials (Hi-GEM) Research Center, from The Featured Areas Research Center Program within the framework of the Higher Education Sprout Project by the Ministry of Education (MOE) and Ministry of Science and Technology (MOST 110-2221-E-006 -112 -MY3), Taiwan.

Appendix A. Supplementary data

Supplementary data to this article can be found online at https://doi.org/10.1016/j.vacuum.2022.111414.

References

[1] L.F. Alves, R.C. Gomes, P. Lefranc, R.d.A. Pegado, P.-O. Jeannin, B.A. Luciano, et al., SIC power devices in power electronics: an overview, in: Brazilian Power Electronics Conference, COBEP), 2017, pp. 1–8, 2017.
[2] M. Östling, R. Ghandi, C.-M. Zetterling, SiC power devices—present status, applications and future perspective, in: IEEE 23rd International Symposium on Power Semiconductor Devices and ICs, 2011, pp. 10–15, 2011.
[3] M. Willander, M. Friesel, Q.-u. Wahab, B. Straumal, Silicon carbide and diamond for high temperature device applications, J. Mater. Sci. Mater. Electron. 17 (2006) 1–25.
[4] M. St G, R. Glass, H. Hobgood, V. Tsvetkov, M. Brady, D. Henshall, et al., The status of SiC bulk growth from an industrial point of view, J. Cryst. Growth 211 (2000) 325–332.
[5] S. Lin, Z. Chen, B. Liu, L. Li, X. Feng, Identification and control of SiC polytypes in PVT method, J. Mater. Sci. Mater. Electron. 21 (2010) 326–330.
[6] D. Hofmann, R. Eckstein, M. Kölbl, Y. Makarov, M. St G, E. Schmitt, et al., SiC-bulk growth by physical-vapor transport and its global modelling, J. Cryst. Growth 174 (1997) 669–674.
[7] S.Y. Hsiao, H.L. Lin, W.H. Lee, W.L. Tsai, K.M. Chiang, W.Y. Liao, et al., Efficient all-vacuum deposited perovskite solar cells by controlling reagent partial pressure in high vacuum, Adv. Mater. 28 (2016) 7013–7019.
[8] S. Dmitriev, Nanosensors engineering: I. structurally modulated sno2 nanowires, Int. J. Smart Sens. Intell. Syst. 3 (2017).
[9] C.-G. Kuo, H.-H. Huang, C.-F. Yang, Effects of the oxygen pressure on the crystalline orientation and strains of YSZ thin films prepared by E-beam PVD, Ceram. Int. 37 (2011) 2037–2041.
[10] L. Zhao, Surface defects in 4H-SiC homoepitaxial layers, Nanotechnol. Prec. Eng. 3 (2020) 229–234.
[11] J. Lento, L. Torpo, T.E. Staab, R. Nieminen, Self-interstitials in 3C-SiC, J. Phys. Condens. Matter 16 (2004) 1053.
[12] M. Chandrashekhar, I. Chowdhury, P. Kaminski, R. Kozlowski, P. Klein, T. Sudarshan, High purity semi-insulating 4H-SiC epitaxial layers by defect-competition epitaxy: controlling Si vacancies, APEX 5 (2012), 025502.
[13] A.A. Alao, W.-D. Hsu, Kinetics and thermodynamics of silicon carbide physical vapor transport reactions: a quantum chemistry and kinetic Monte Carlo approach, Chem. Phys. 554 (2022), 111421.
[14] H.C. Barshilia, A. Ananth, J. Khan, G. Srinivas, Ar+ H2 plasma etching for improved adhesion of PVD coatings on steel substrates, Vacuum 86 (2012) 1165–1173.
[15] D.-K. Kim, K.-S. Jeong, Y.-S. Kang, H.-K. Kang, S.W. Cho, S.-O. Kim, et al., Controlling the defects and transition layer in SiO2 films grown on 4H-SiC via direct plasma-assisted oxidation, Sci. Rep. 6 (2016) 1–11.
[16] A. Kubota, M. Yoshimura, S. Fukuyama, C. Iwamoto, M. Touge, Planarization of C-face 4H-SiC substrate using Fe particles and hydrogen peroxide solution, Precis. Eng. 36 (2012) 137–140.
[18] Q. Lu, Growth, Dielectrics Properties, and Reliability of High-K Thin Films Grown on Si and Ge Substrates, The University of Liverpool, United Kingdom), 2017.
[19] 조영진, Interface Sulfur Passivation for Advanced MOSFETs with High Mobility Channel Materials, 서울대학교 대학원, 2015.
[20] K. Pandey, New π-bonded chain model for Si (111)-(2× 1) surface, Phys. Rev. Lett. 47 (1981) 1913.
[21] J. Olander, K. Larsson, Influence of adsorbed species on the reconstruction of 4H−SiC (0001) surfaces, J. Phys. Chem. B 105 (2001) 7619–7623.
[22] K. Jeganathan, M. Shimuzu, H. Okumura, F. Hirose, S. Nishizawa, Initial stage of GaN nucleation on $\sqrt{3}\times\sqrt{3}$R30°-Ga reconstructed 4H-SiC (0001) Si by molecular-beam epitaxy, Surf. Sci. 527 (2003) L197–L202.
[23] U. Starke, M. Tallarida, A. Kumar, K. Horn, O. Seifarth, L. Kipp, Reconstruction of cleaved 6H-SiC surfaces, in: Materials Science Forum, 2004, pp. 391–394.
[24] T. Kaneko, T. Yamasaki, N. Tajima, T. Ohno, First-principles study on reconstruction of 4H-SiC (0001) and (000$\bar{1}$), Surf. Sci. 647 (2016) 45–50.
[25] H. Jagodzinski, Eindimensionale Fehlordnung in Kristallen und ihr Einfluss auf die Röntgeninterferenzen. I. Berechnung des Fehlordnungsgrades aus den Röntgenintensitäten, Acta Crystallogr. 2 (1949) 201–207.
[26] P. Hohenberg, W. Kohn, Inhomogeneous electron gas, Phys. Rev. 136 (1964) B864.
[27] W.a.S. Kohn, Self-consistent equations including exchange and correlation effects, L.J. Phys. Rev. 140 (1965) A1133.
[28] J.P. Perdew, K. Burke, M. Ernzerhof, Generalized gradient approximation made simple, Phys. Rev. Lett. 77 (1996) 3865.
[29] P.E. Blöchl, Projector augmented-wave method, Phys. Rev. B 50 (1994) 17953–17979.
[30] J.D. Kresse G, From ultrasoft pseudopotentials to the projector augmented-wave method, Phys. Rev. B 59 (1999) 1758.
[31] John P. Perdew, Kieron Burke, Matthias Ernzerhof, Generalized gradient approximation made simple, Phys. Rev. Lett. 77 (1996) 3865–3868, https://doi.org/10.1103/PhysRevLett.77.3865.
[32] J. Borysiuk, J. Sołtys, R. Bożek, J. Piechota, S. Krukowski, W. Strupiński, J. M. Baranowski, R. Stępniewski, Role of structure of C-terminated 4 H-SiC (000 1$\bar{}$) surface in growth of graphene layers: transmission electron microscopy and density functional theory studies, Phys. Rev. B 85 (2012), 045426.
[33] T. Kobayashi, K. Harada, Y. Kumagai, F. Oba, Y.I. Matsushita, Native point defects and carbon clusters in 4H-SiC: a hybrid functional study, J. Appl. Phys. 125 (2019), 125701.
[34] Michael E. Levinshtein, Sergey L. Rumyantsev, Michael S. Shur, M.S. Shur (Eds.), Properties of Advanced Semiconductor Materials GaN, AlN, SiC, BN, SiC, SiGe, John Wiley & Sons, Inc., New York, 2001.
[35] J.D.P. Hendrik J Monkhorst, Special points for Brillouin-zone integration, Phys. Rev. B 13 (1976) 5188.
[36] P. Sukkaew, O. Danielsson, O. Kordina, E. Janzen, L. Ojamae, Ab initio study of growth mechanism of 4H–SiC: adsorption and surface reaction of C2H2, C2H4, CH4, and CH3, J. Phys. Chem. C 121 (2017) 1249–1256.
[37] K. Reuter, M. Scheffler, First-principles kinetic Monte Carlo simulations for heterogeneous catalysis: application to the CO oxidation at Ru O 2 (110), Phys. Rev. B 73 (2006), 045433.
[38] Z. Insepov, A. Zhankadamova, Molecular dynamics calculation of the sticking coefficient of gases to surfaces, Z. Physik D Atoms, Mol. Clust. 20 (1991) 145–146.
[39] L. Schwaederlé, P. Brault, C. Rond, A. Gicquel, Molecular dynamics calculations of CH3 sticking coefficient onto diamond surfaces, Plasma Process. Polym. 12 (2015) 764–770.
[40] K.C. Pandey, Phys. Rev. Lett. 47 (1981) 1913.
[41] K. Pandey, Reconstruction of semiconductor surfaces: buckling, ionicity, and π-bonded chains, Phys. Rev. Lett. 49 (1982) 223.
[42] G. Froudakis, A. Zdetsis, M. Mühlhäuser, B. Engels, S.D. Peyerimhoff, A comparative ab initio study of the Si2C4, Si3C3, and Si4C2 clusters, J. Chem. Phys. 101 (1994) 6790–6799.
[43] P. Pradhan, A.K. Ray, A density functional study of the structures and energetics of small hetero-atomic silicon–carbon nanoclusters, J. Mol. Struct.: THEOCHEM 716 (2005) 109–130.
[44] S. Kyushin, Y. Kurosaki, K. Otsuka, H. Imai, S. Ishida, T. Kyomen, et al., Silicon–silicon π single bond, Nat. Commun. 11 (2020) 1–7.
[45] J. Wagler, U. Böhme, G. Roewer, Activation of a Si− Si bond by hypercoordination: cleavage of a disilane and formation of a Si− C bond, Organometallics 23 (2004) 6066–6069.
[46] M.N. Huda, A.K. Ray, Theoretical study of SiC nanostructures: current status and a new theoretical approach, J. Comput. Theor. Nanosci. 9 (2012) 1881–1905.

[47] Y. Ishigaki, T. Shimajiri, T. Takeda, R. Katoono, T. Suzuki, Longest C–C single bond among neutral hydrocarbons with a bond length beyond 1.8 Å, Chem 4 (2018) 795–806.
[48] Wikipedia, in Silicon Carbide, ed: Wikimedia.
[49] K. Ariyawong, Process Modeling for the Growth of SiC Using PVT and TSSG Methods, Université Grenoble Alpes, 2015.
[50] M.W. Chase Jr., NIST-JANAF thermochemical tables, J. Phys. Chem. Ref. Data, Monograph 9 (1998).
[51] S. Lilov, Study of the equilibrium processes in the gas phase during silicon carbide sublimation, Mater. Sci. Eng., B 21 (1993) 65–69.
[52] P. Rocabois, C. Chatillon, C. Bernard, Thermodynamics of the Si-C system I. mass spectrometry studies of the condensed phases at high temperature, High. Temp. - High. Press. 27 (1995) 3–23.
[53] P. Rocabois, C. Chatillon, C. Bernard, F. Genet, Thermodynamics of the Si-C system II. Mass spectrometric determination of the enthalpies of formation of molecules in the gaseous phase, High. Temp. - High. Press. 27 (1995) 25–39.
[54] S. SGTE, "38402 Saint Martin d'Heres," ed: (France).
[55] J. Lacaze, B. Sundman, An assessment of the Fe-C-Si system, Metall. Trans. A 22 (1991) 2211–2223.
[56] M. Amsler, S. Botti, M.A. Marques, T.J. Lenosky, S. Goedecker, Low-density silicon allotropes for photovoltaic applications, Phys. Rev. B 92 (2015), 014101.
[57] A. Evans, M. Polanyi, Calculation of steric hindrance, Nature 149 (1942), 608-608.
[58] WebElements (January, Silicon: radii of atoms and ions, Available: https://www.webelements.com/silicon/atom_sizes.html.
[59] WebElements (January, Carbon: radii of atoms and ions, Available: https://www.webelements.com/carbon/atom_sizes.html.
[60] M. Selder, L. Kadinski, Y. Makarov, F. Durst, P. Wellmann, T. Straubinger, M. Ramm, Global numerical simulation of heat and mass transfer for SiC bulk crystal growth by PVT, J. Cryst. Growth 211 (2000) 333–338.
[61] E. Tymicki, K. Grasza, R. Diduszko, R. Bożek, M. Gała, Initial stages of SiC crystal growth by PVT method, Cryst. Res. Technol.: J. Exp. Ind. Crystallogr. 42 (2007) 1232–1236.
[62] E.Y. Tupitsyn, A. Arulchakkaravarthi, R.V. Drachev, T.S. Sudarshan, Controllable 6H-SiC to 4H-SiC polytype transformation during PVT growth, J. Cryst. Growth 299 (2007) 70–76.
[63] Q.S. Chen, J.Y. Yan, V. Prasad, Application of flow-kinetics model to the PVT growth of SiC crystals, J. Cryst. Growth 303 (2007) 357–361.
[64] D.L. Barrett, J.P. McHugh, H.M. Hobgood, R.H. Hopkins, P.G. McMullin, R. C. Clarke, W.J. Choyke, Growth of large SiC single crystals, J. Cryst. Growth 128 (1993) 358–362.